

# Heterogeneous Interactions between SO<sub>2</sub> and Organic Peroxides in Submicron Aerosol

Shunyao Wang<sup>1</sup>, Tengyu Liu<sup>2</sup>, Jinmyung Jang<sup>1</sup>,  
Jonathan P.D. Abbott<sup>2</sup> and Arthur W.H. Chan<sup>1\*</sup>

<sup>1</sup> Department of Chemical Engineering and Applied Chemistry, University of Toronto,  
Toronto, Ontario, M5S 3E5, Canada

<sup>2</sup> Department of Chemistry, University of Toronto, Toronto, Ontario, M5S 3H6, Canada

21 \*Correspondence to: Arthur W.H. Chan (arthurwh.chan@utoronto.ca)

22 **Abstract**

23 Atmospheric models often underestimate particulate sulfate, a major component in ambient  
24 aerosol, suggesting missing sulfate formation mechanisms in the models. Heterogeneous  
25 reactions between  $\text{SO}_2$  and aerosol play an important role in particulate sulfate formation and its  
26 physicochemical evolution. Here we study the reactive uptake kinetics of  $\text{SO}_2$  onto aerosol  
27 containing organic peroxides. We present chamber studies of  $\text{SO}_2$  reactive uptake performed  
28 under different relative humidities (RH), particulate peroxide contents, peroxide types, and  
29 aerosol acidities. Using different model organic peroxides mixed with ammonium sulfate  
30 particles,  $\text{SO}_2$  uptake coefficient ( $\gamma_{\text{SO}_2}$ ) was found to be exponentially dependent on RH.  $\gamma_{\text{SO}_2}$   
31 increases from  $10^{-3}$  at RH 25% to  $10^{-2}$  at RH 71% as measured for an organic peroxide with  
32 multiple O-O groups. Under similar conditions, the kinetics in this study were found to be  
33 structurally dependent: organic peroxides with multiple peroxide groups have a higher  $\gamma_{\text{SO}_2}$  than  
34 those with only one peroxide group, consistent with the reactivity trend observed previously in  
35 the aqueous phase. In addition,  $\gamma_{\text{SO}_2}$  is linearly related to particle-phase peroxide content, which  
36 in turn depends on gas-particle partitioning of organic peroxides. Aerosol acidity plays a  
37 complex role in determining  $\text{SO}_2$  uptake rate, influenced by the effective Henry's Law constant  
38 of  $\text{SO}_2$  and the condensed phase kinetics of the peroxide- $\text{SO}_2$  reaction in the highly concentrated  
39 aerosol phase. These uptake coefficients are consistently higher than those calculated from the  
40 reaction kinetics in the bulk aqueous phase, and we show experimental evidence suggesting that  
41 other factors, such as particle-phase ionic strength, can play an essential role in determining the  
42 uptake kinetics.  $\gamma_{\text{SO}_2}$  for different types of secondary organic aerosol (SOA) were measured to be  
43 on the order of  $10^{-4}$ . Overall, this study provides quantitative evidence of the multiphase

44 reactions between  $\text{SO}_2$  and organic peroxides, highlighting the important factors that govern the  
45 uptake kinetics.

46 **Introduction**

47 Sulfate and organic compounds are ubiquitous particulate components in both polluted and  
48 pristine environments (Chen et al., 2009;Andreae et al., 2018;He et al., 2011;Sun et al.,  
49 2013;Huang et al., 2014), with important implications for public health and global climate  
50 (Hallquist et al., 2009). Particulate sulfate can form via S(IV) oxidation by OH radicals in the gas  
51 phase and via oxidation in cloud water, fog droplets or the aerosol aqueous phase, including by  
52  $\text{H}_2\text{O}_2$ ,  $\text{O}_2$  (catalyzed by transition metals),  $\text{O}_3$ ,  $\text{NO}_2$  and small organic peroxides (methyl  
53 hydroperoxide and peroxyacetic acid) (Seinfeld and Pandis, 2012). However, atmospheric  
54 models tend to underestimate particulate sulfate production on both global (Tie et al., 2001;Yang  
55 et al., 2017;Fairlie et al., 2010) and regional scales, especially during heavy haze episodes (Wang  
56 et al., 2014;Zheng et al., 2015;Sha et al., 2019;Gao et al., 2016;Li et al., 2017;Huang et al.,  
57 2019), suggesting that the overall kinetics may be underestimated and/or important mechanisms  
58 may be missing in models.

59 To reconcile these differences, studies have investigated novel reaction mechanisms of sulfate  
60 formation. Stabilized Criegee intermediates (sCIs) were hypothesized to oxidize  $\text{SO}_2$  rapidly and  
61 potentially serve as an important source of ambient sulfate (Mauldin et al., 2012). In the work by  
62 Newland et al. (2015) and Nguyen et al. (2016), this sCI pathway was shown to play a minor role  
63 in sulfate formation. More recently, when Liu et al. (2019) applied this mechanism and kinetics  
64 to a source-oriented WRF-Chem model, the sCIs pathway was found to only account for at most  
65 9% of the total particulate sulfate. Reactive nitrogen species (such as  $\text{NO}_2$ ) have also been  
66 proposed as a dominant sulfate formation pathway when aerosol pH was estimated to be 5-6 in

67 Cheng et al. (2016) and close to 7 in Wang et al. (2016) under severe haze scenarios. While such  
68 high aerosol pH is not substantiated by some thermodynamic modeling results, which concluded  
69 that pH ranges between 4 and 5 in polluted regions (Song et al., 2018;Guo et al., 2017), other  
70 studies that highlighted the roles of ammonia and dust found aerosol pH could be higher than 6  
71 (Shi et al., 2017; Ding et al., 2019). Furthermore, higher aerosol water content and PM mass  
72 concentration in polluted areas have been shown to enhance aerosol pH via a multiphase  
73 buffering process (Zheng et al., 2020). Meanwhile, a recent modeling study incorporating this  
74 heterogeneous NO<sub>x</sub> mechanism still exhibited a discrepancy of 20% between the predicted and  
75 observed sulfate, indicating the possibility of unknown mechanisms (Huang et al., 2019). Other  
76 factors may play a role in enhancing the particle-phase sulfate formation rates. Chen et al. (2019)  
77 investigated the synergistic effects of NO<sub>2</sub> and NH<sub>3</sub> on sulfate formation, and found that the rate  
78 of this reaction can be enhanced by the high ionic strength in the particle phase. This  
79 enhancement effect by solute strength on sulfate formation was also investigated for the H<sub>2</sub>O<sub>2</sub>  
80 pathway in aerosol liquid water. Liu et al. (2020) found ionic strength and general acid-catalyzed  
81 mechanisms can cause the S(VI) formation rate to be nearly 50 times faster in aerosol phase than  
82 in dilute solutions. On the other hand, during the severe haze episodes in China (Li et al., 2020;  
83 Guo et al., 2017), transition metal ion (TMI) catalysis of SO<sub>2</sub> oxidation by O<sub>2</sub> can be  
84 significantly suppressed in the aerosol phase due to high ionic strength (Liu et al., 2020;Cheng et  
85 al., 2016; Su et al., 2020).  
86 In addition to high solute strength, submicron aerosol is also rich in organic compounds (Jimenez  
87 et al., 2009;Hallquist et al., 2009). In recent years, many studies have investigated the potential  
88 role of heterogeneous interactions between SO<sub>2</sub> and organic aerosol on particulate sulfate  
89 formation. Song et al. (2019) found heterogeneous oxidation of hydroxymethanesulfonate

90 (HMS) by OH can trigger rapid sulfate formation. Wang et al. (2020) studied photosensitizers in  
91 ambient particles and found this pathway could be essential under specific light conditions.  
92 Recent studies found reactive intermediates from isoprene oxidation (Huang et al., 2019) and  
93 benzoic acid (Huang et al., 2020), can yield a variety of organosulfur species upon catalysis by  
94 TMI. Other studies have also investigated the interactions between secondary organic aerosol  
95 (SOA) and SO<sub>2</sub>. Field observations found that ambient sulfate abundance is highly correlated  
96 with SOA formation (Yee et al., 2020; Xu et al., 2015). Liu et al. (2019) found that SO<sub>2</sub> enhances  
97 SOA formation and average carbon oxidation state during methoxyphenol photooxidation. By  
98 performing chamber experiments with limonene SOA formation in the presence of SO<sub>2</sub>, Ye et al.  
99 (2018) also observed significant SO<sub>2</sub> decay along with increased SOA yields and carbon  
100 oxidation state, proposing that organic peroxides in SOA may be the key reactive intermediates  
101 for SO<sub>2</sub> oxidation.

102 Organic peroxides are key intermediates for aerosol formation and ubiquitously exist in many  
103 SOA systems (Hallquist et al., 2009; Bianchi et al., 2019). Numerous studies have reported  
104 peroxide content of 20-60% for isoprene and monoterpene derived SOA (Surratt et al., 2006; Ng  
105 et al., 2008; Ye et al., 2018; Epstein et al., 2014). A significant fraction of organic peroxide (30%-  
106 50%) has also been found in naphthalene-derived SOA under low/high NO<sub>x</sub> conditions  
107 (Kautzman et al., 2009). Using model simulations, Bonn et al. (2004) found organic  
108 hydroperoxides can account for up to 60% of global SOA. The aqueous phase reaction kinetics  
109 between organic peroxides and dissolved SO<sub>2</sub> have been explored in previous studies (Lind et al.,  
110 1987; Gunz and Hoffmann, 1990; Wang et al., 2019; Dovrou et al., 2019; Yao et al., 2019). The  
111 second order reaction rate constants for organic peroxides in SOA (Dovrou et al., 2019; Yao et  
112 al., 2019) and S(IV) were measured to be on the order of 10<sup>2</sup>-10<sup>3</sup> M<sup>-1</sup> s<sup>-1</sup>, which are within the

113 range of those measured for commercially available organic peroxides (Wang et al., 2019) and  
114 small organic peroxides (Lind et al., 1987). Yao et al. (2019) quantified the reactive uptake  
115 coefficient of  $\text{SO}_2$  ( $\gamma_{\text{SO}_2}$ ) onto  $\alpha$ -pinene SOA to be on the order of  $10^{-4}$ - $10^{-3}$ , which is positively  
116 dependent on RH and inferred particle-phase peroxide content. These reactions are also linked to  
117 the formation of organosulfates (Wang et al., 2019). Both inorganic sulfate (85-90%) and  
118 organosulfates (10-15%) were observed as products of  $\text{SO}_2$  reactive uptake onto SOA (Yao et al.,  
119 2019).

120 Given the potential significance of  $\text{SO}_2$  reactive uptake in particulate sulfate formation, a more  
121 in-depth study is needed to determine the important factors that govern the heterogeneous  
122 kinetics of  $\text{SO}_2$  onto organic peroxide containing aerosol. In this study, we measured  $\gamma_{\text{SO}_2}$  for two  
123 categories of aerosol: 1. Model organic peroxides mixed with ammonium sulfate or malonic acid  
124 and 2. SOA from a few representative biogenic and anthropogenic precursors. The impacts of  
125 RH, peroxide type, peroxide content, and condensed phase pH on  $\text{SO}_2$  reactive uptake were  
126 evaluated systematically with the goal of better understanding atmospheric multiphase sulfate  
127 formation.

128

## 129 **2. Methods**

130 The reactive uptake of  $\text{SO}_2$  onto peroxide-containing particles was studied in a 1  $\text{m}^3$  Teflon  
131 chamber under ambient temperature and pressure. In brief, generated particles and  $\text{SO}_2$  were  
132 introduced into the chamber separately. The consumption of  $\text{SO}_2$ , changes in particle size  
133 distribution and chemical composition were monitored to estimate the reactive uptake  
134 coefficients. Particles were also collected on filters for offline chemical characterization.

135

136 **2.1 Seed aerosol generation**

137 In this work, two types of aerosol were used to investigate the uptake of  $\text{SO}_2$ . The first is  
138 ammonium sulfate or malonic acid mixed with model organic peroxides (Fig. S1). In this first set  
139 of experiments, an aerosol atomizer (Model 3076, TSI Inc., USA) was used to generate aqueous  
140 particles from dilute solution. Each solution consists of ammonium sulfate ( $\geq 99\%$ , Sigma-  
141 Aldrich) or malonic acid (99%, Sigma-Aldrich) and a model organic peroxide in ultrapure water  
142 (HPLC grade, Fisher Chemical). For the experiments investigating the relationship between  $\gamma_{\text{SO}_2}$   
143 and peroxide type (Expt. 2-14, Table S1), different commercially available organic peroxides  
144 were used, including tert-butyl hydroperoxide (70 wt. % in water, Sigma-Aldrich), cumene  
145 hydroperoxide (80 wt. % in water, Sigma-Aldrich), and 2-butanone peroxide (40% wt. % in  
146 water, Sigma-Aldrich). The molar ratio of organic peroxide to ammonium sulfate in the  
147 atomizing solution was 2:1 with the aim of being atmospherically relevant (corresponding to  
148 maximum particulate peroxide molar fraction of 66% and mass fraction of approximately 50-  
149 70% if all the organic peroxides were assumed to remain in the particle phase). This ratio was  
150 used as a proxy for total peroxide content in both gas and particle phase relative to that of  
151 ammonium sulfate upon atomization. For the experiments studying the relationship between  $\gamma_{\text{SO}_2}$   
152 and particle-phase peroxide content, the molar ratio of organic peroxide to ammonium sulfate  
153 (Expt. 10-12, 15-18, Table S1) in the solution was adjusted to be 0.02, 0.2, 1, 2, and 4,  
154 respectively. In experiments where malonic acid was used (Expt. 19-22, Table S1), molar ratios  
155 of 0.2, 1, 2, and 4 were adopted. For measuring  $\gamma_{\text{SO}_2}$  with different aerosol pH (Expt. 17, 23-25,  
156 Table S1), different amounts of HCl (37%, Sigma-Aldrich) were added into the solution (0,  
157 0.00002 M, 0.0001 M, 0.001 M HCl) prior to atomization. The initial pH of aerosol (2.5, 2.2,  
158 1.6, 1, respectively) were modeled using E-AIM III model (Clegg et al., 1998) based on the

159 initial molar ratios of inorganic species ( $\text{H}^+$ ,  $\text{NH}_4^+$ ,  $\text{SO}_4^{2-}$ ,  $\text{Cl}^-$ ) in the atomizing solution and  
160 measured RH (around 50%). The atomized particles were flowed into the chamber without  
161 drying, and therefore assumed to remain deliquesced under the range of RH we studied. Expt. 2-  
162 14 (Table S1) also represent those where the relationship between  $\gamma_{\text{SO}_2}$  and RH conditions were  
163 studied.

164 In the second set of experiments, the uptake of  $\text{SO}_2$  onto SOA was investigated (Fig. S2, Expt.  
165 26-28, Table S1). A custom-built 10 L quartz oxidation flow reactor was used to produce SOA  
166 (Ye et al., 2016) from different hydrocarbon precursors. In this work, we studied SOA formed  
167 from toluene photooxidation, limonene ozonolysis and  $\alpha$ -pinene ozonolysis, 3 of the most  
168 commonly studied SOA systems (Ng et al., 2007; Hildebrandt et al., 2009; Hartz et al.,  
169 2005; Varutbangkul et al., 2006). Toluene (analytical standard, Sigma Aldrich) was injected  
170 continuously into zero air flow by a syringe (1000 mL, Hamilton) installed on a syringe pump  
171 (KDS Legato100) to achieve an initial concentration of 0.5 ppm. Limonene (Sigma-Aldrich,  
172 97 %) and  $\alpha$ -pinene (Sigma-Aldrich, 98 %) were pre-dissolved in cyclohexane (Sigma-Aldrich,  
173 99.5 %) with a volumetric ratio of 1: 1500 and 1: 500 to ensure that OH formed from limonene  
174 or  $\alpha$ -pinene ozonolysis is scavenged by cyclohexane, estimated based on the rate constants  
175 (Atkinson and Arey, 2003). The initial steady-state concentrations of limonene and  $\alpha$ -pinene  
176 were controlled to be around 2 ppm and 1 ppm entering the flow tube.  $\text{O}_3$ , used as the oxidant  
177 (for limonene and  $\alpha$ -pinene) or the OH precursor (for toluene), was generated by passing 0.5 L  
178  $\text{min}^{-1}$  pure oxygen (99.6 %, Linde, Mississauga, Canada) through an  $\text{O}_3$  generator (no.  
179 97006601, UVP, Cambridge, UK). Humidified air was produced by bubbling zero air through a  
180 custom-made humidifier at a flow rate of 1 L  $\text{min}^{-1}$ . The photolysis of  $\text{O}_3$  produces  $\text{O} (^1\text{D})$ ,  
181 which reacts with water vapour to produce  $\cdot\text{OH}$  with illumination from the 254 nm UV lamps

182 (UVP, Cambridge, UK) to initiate the photooxidation of toluene. The average residence time  
183 inside the flow tube was controlled to be around 5 minutes. A gas chromatography–flame  
184 ionization detector (GC-FID, model 8610C, SRI Instruments Inc., LV, USA) equipped with a  
185 Tenax® TA trap was used to monitor the concentration of hydrocarbon precursors at the  
186 inlet/outlet of the flow reactor. In all cases, the O<sub>3</sub> concentration was maintained to be at least 10  
187 times higher than that of the hydrocarbon. Temperature and relative humidity were monitored by  
188 an Omega HX94C RH/T transmitter. Particle size distribution and volume concentration were  
189 monitored using a custom-built scanning mobility particle sizer (SMPS), which is a combination  
190 of a differential mobility analyzer column (DMA, model 3081, TSI, Shoreview, MN, USA) with  
191 flow controls and a condensation particle counter (CPC, model 3772, TSI, Shoreview, MN,  
192 USA).

193

## 194 **2.2 Quantification of $\gamma_{SO_2}$**

195 Prior to each experiment, the chamber was flushed by purified air overnight with a flow rate of  
196 25 L min<sup>-1</sup> until particle number concentration was less than 5 cm<sup>-3</sup> and SO<sub>2</sub> was less than 1 ppb.  
197 To adjust RH, the chamber was humidified by passing purified air through a custom-built  
198 humidifier filled with ultra-pure water. For experiments with atomized ammonium sulfate or  
199 malonic acid, SO<sub>2</sub> was injected into the chamber prior to the introduction of particles. For  
200 experiments studying  $\gamma_{SO_2}$  onto SOA, aerosol generated from the flow tube was injected into the  
201 Teflon chamber continuously after passing through an O<sub>3</sub> denuder (Ozone Solutions, Iowa, USA)  
202 to achieve specific aerosol concentration inside the chamber prior to SO<sub>2</sub> addition. SO<sub>2</sub> mixing  
203 ratio in the chamber during each experiment was continuously monitored using an SO<sub>2</sub> analyzer  
204 (Model 43i, Thermo Scientific). The initial mixing ratio of SO<sub>2</sub> in each experiment was

205 controlled to be around 200 ppb. Aerosol size distribution was monitored by SMPS. The reactive  
206 uptake coefficient of SO<sub>2</sub> was calculated by integrating the following equation:

207 
$$-\frac{d[SO_2]}{dt} = \frac{1}{4} \gamma_{SO_2} A \bar{c} [SO_2] \quad (1)$$

208  
209 Where [SO<sub>2</sub>] is the SO<sub>2</sub> mixing ratio (ppb) monitored by the SO<sub>2</sub> analyzer; A is the average  
210 surface area concentration ( $\mu\text{m}^2 \text{ cm}^{-3}$ ) derived from the particle size distribution measured by  
211 SMPS;  $\bar{c}$  represents the mean molecular velocity ( $\text{cm s}^{-1}$ ) of SO<sub>2</sub>.  $d[SO_2]/dt$  is solved over the  
212 initial SO<sub>2</sub> decay, such that the peroxide concentration in the aerosol liquid phase is assumed to  
213 be constant and pseudo-first order kinetics can be applied (Abbatt et al., 2012; Thornton et al.,  
214 2003). A summary of all the measured  $\gamma_{SO_2}$  can be found in Table S1. Typical evolution of  
215 monitored species can be seen in Fig.1. Control experiments were performed in order to rule out  
216 other potential factors (e.g. SO<sub>2</sub> loss in the in-line filter in front of the SO<sub>2</sub> analyzer, interferences  
217 inside the SO<sub>2</sub> analyzer, chamber wall losses, SO<sub>2</sub> uptake onto wet ammonium sulfate, gas-phase  
218 reaction of SO<sub>2</sub> with peroxide vapour) that may contribute to the SO<sub>2</sub> decay observed during the  
219  $\gamma_{SO_2}$  measurement inside the chamber (Fig. S3-S6). Measurement uncertainty and precision of  
220  $\gamma_{SO_2}$  in this study can be found in Table S1. Also, we observed there was SO<sub>2</sub> repartitioning from  
221 the humid chamber wall in the presence of organic peroxide under high RH (Fig. S6b, RH 74%).  
222 The observed SO<sub>2</sub> repartitioning rate was then applied to correct the  $\gamma_{SO_2}$  measured under high  
223 RH conditions (above 70%, Expt.14), and this correction amounts to a 40% increase in  
224 calculated  $\gamma_{SO_2}$ .

225

226 **2.3 Offline peroxide quantification**

227 Aerosol was collected onto 47 mm PTFE (polytetrafluoroethylene) filters with 0.2  $\mu\text{m}$  pore size  
228 (Whatman®, GE Healthcare) from the chamber by a diaphragm pump (KNF Neuberger Inc., USA)

229 for offline chemical analysis. The total particulate peroxide content ( $\text{H}_2\text{O}_2$ ,  $\text{ROOH}$  and  $\text{ROOR}$ ) in  
230 these samples prior to  $\text{SO}_2$  uptake was quantified using the iodometric–spectrophotometric assay  
231 (Docherty et al., 2005).  $\text{I}_2$  produced from the reaction between  $\text{I}^-$  and peroxides can further quickly  
232 combine with the excess amount of  $\text{I}^-$  to form  $\text{I}_3^-$ , which has brown color and absorbs UV-vis at  
233 470nm. The SOA extraction was then aliquoted into a 96-well UV plate (Greiner Bio-One,  
234 Kremsmünster, AT) with  $160 \mu\text{L}$  well $^{-1}$ .  $20 \mu\text{L}$  of formic acid ( $\geq 95\%$ , Sigma-Aldrich) was added  
235 into each well, following by  $20 \mu\text{L}$  potassium iodide (BioUltra,  $\geq 99.5\%$ , Sigma-Aldrich) solution  
236 (dissolved in DI water). The plate was then covered by an adhesive plate sealer (EdgeBio,  
237 Gaithersburg, USA) immediately in order to avoid reagent evaporation and  $\text{O}_2$  oxidation. After  
238 incubation for an hour in the dark, the UV-vis absorption at 470nm was measured using a UV-vis  
239 spectrophotometer (Spectramax 190, Molecular Devices Corporation, Sunnyvale, CA) and then  
240 converted to peroxide concentration using the calibration curve made by tert-butyl hydroperoxide  
241 (70 wt. % in  $\text{H}_2\text{O}$ , Sigma-Aldrich) with a series of concentrations (0-10mM). An average  
242 molecular mass for seed particles (organics + ammonium sulfate) was assumed based on the  
243 chemical composition in order to calculate the molar fraction of total peroxides using the following  
244 equation:

245

$$246 \text{Molar fraction of peroxide} = \frac{N_{\text{peroxide}}}{N_{\text{aerosol}}} = N_{\text{peroxide}} \frac{M_{(\text{NH}_4)_2\text{SO}_4} f_{(\text{NH}_4)_2\text{SO}_4} + M_{\text{peroxide}} f_{\text{peroxide}}}{m_{\text{aerosol}}} \quad (2)$$

247

248 where  $m_{\text{aerosol}}$  is the weighed aerosol mass on the filter;  $M_{(\text{NH}_4)_2\text{SO}_4}$  and  $M_{\text{peroxide}}$  are the  
249 molecular mass of ammonium sulfate and peroxide, respectively;  $f_{(\text{NH}_4)_2\text{SO}_4}$  and  $f_{\text{peroxide}}$  are the  
250 initial molar fraction of ammonium sulfate and peroxide;  $N_{\text{peroxide}}$  and  $N_{\text{aerosol}}$  are the  
251 measured peroxide molar and calculated aerosol molar, respectively. More details about the  
252 iodometric-spectrophotometric procedures were described in previous work (Wang et al., 2018).

253

254 **3 Results and discussion**

255 **3.1 SO<sub>2</sub> uptake and RH**

256 A positive relationship between  $\gamma_{\text{SO}_2}$  and RH (between 25 and 71%) was observed for all types of  
257 organic peroxides studied (Fig. 2). The positive dependence of the reactive uptake coefficient of  
258 water-soluble gaseous species on RH has also been observed in other studies (Thornton et al.,  
259 2003;Griffiths et al., 2009;Zhao et al., 2017;Zhang et al., 2019). Recently, the uptake behavior of  
260 SO<sub>2</sub> onto soot, mineral dust and SOA were also shown to positively depend on RH (Zhang et al.,  
261 2019;Zhao et al., 2017;Yao et al., 2019).

262 It is also noteworthy that an exponential dependence of SO<sub>2</sub> reactive uptake coefficient on RH  
263 was observed in our study.  $\gamma_{\text{SO}_2}$  increases with increased relative humidity, which could even be  
264 more significant under high RH regime. This is consistent with previous laboratory studies that  
265 measured the reactive uptake coefficient of SO<sub>2</sub> onto aerosol to be exponentially dependent on  
266 RH (Zhang et al., 2019;Yao et al., 2019). Additionally, multiple field campaigns have observed  
267 significant correlation between particulate sulfate formation and ambient RH (Song et al.,  
268 2019;Sun et al., 2013;Huang et al., 2020). Sun et al. (2013) observed faster sulfate formation rate  
269 under humid conditions, proposing a significant impact of aerosol liquid water on sulfate  
270 production during wintertime in Beijing. Zheng et al. (2015) reported a notably higher SOR  
271 (molar ratio of sulfate to the sum of sulfate and SO<sub>2</sub>) during wet period (RH>50%), indicating  
272 the importance of heterogeneous reactions to the secondary sulfur transformation with abundant  
273 aerosol water content under humid conditions. In a recent study by Song et al. (2019), the rapid  
274 sulfate formation rate observed under high RH conditions was found to be significantly higher  
275 than atmospheric modeling results implemented with homogeneous SO<sub>2</sub> oxidation pathways,

276 which was later attributed to heterogeneous sulfate formation mechanisms. Multiple mechanisms  
277 can potentially explain this observed  $\gamma_{\text{SO}_2}$ -RH dependence. An enhanced relative humidity would  
278 result in a nonlinear increase of aerosol water content, which can lead to more  $\text{SO}_2$  dissolved in  
279 the aerosol aqueous phase (Seinfeld and Pandis, 2012). It should be noted that while the relative  
280 humidity is varied systematically in these experiments, the relationship is more complex since  
281 RH also affects other aerosol properties which can affect the uptake kinetics in turn. For  
282 example, a higher aerosol liquid water content could dilute protons and thus lower the aerosol  
283 acidity. In a study by Laskin et al. (2003), an enhanced uptake of  $\text{SO}_2$  onto sea-salt particles was  
284 observed with an increased aerosol alkalinity at high pH range.

285

### 286 **3.2 Dependence of $\text{SO}_2$ uptake on peroxide content and type**

287 As expected, the measured uptake rate of  $\text{SO}_2$  is dependent on the particulate peroxide content in  
288 the current study. Fig. 3 shows that  $\gamma_{\text{SO}_2}$  is linearly proportional to the amount of particulate  
289 peroxide for aerosol with similar volume-to-surface ratios and containing the same type of  
290 organic peroxides. This positive relationship between  $\gamma_{\text{SO}_2}$  and condensed phase peroxide content  
291 has also been inferred from experiments of  $\text{SO}_2$  uptake onto  $\alpha$ -pinene SOA (Yao et al., 2019),  
292 where the peroxide content in  $\alpha$ -pinene SOA was varied indirectly by introducing NO and  
293 adjusting the branching ratio of the peroxide-yielding  $\text{RO}_2 + \text{HO}_2 / \text{RO}_2$  pathway.  
294 In addition to the amount of peroxide injected, the particulate fraction of organic peroxide  
295 available for heterogeneous reaction is also influenced by gas-particle partitioning. As indicated  
296 in Fig. 2, the reactive uptake coefficients of different organic peroxides vary amongst each other  
297 by about an order of magnitude in the range of RH studied, despite the same amounts of peroxide  
298 relative to ammonium sulfate initially in the atomizing solution. Based on our previous work

299 (Wang et al., 2019), the aqueous-phase rate constants for these organic peroxides with dissolved  
300 S(IV) only vary by a factor of 2-3 and therefore cannot fully explain the observed difference in  
301 uptake rates. Since vapour pressure vary considerably among the different peroxides in the  
302 present study, gas-particle partitioning is likely to influence the amount of peroxide in the  
303 particle phase that react with dissolved SO<sub>2</sub>. The relative particulate peroxide content on filters  
304 of the three peroxides collected from chamber experiments under RH 50% without SO<sub>2</sub> uptake  
305 were measured by the offline KI method (Fig. S7). Although the initial ratio of organic peroxide  
306 to ammonium sulfate in the atomizing solution was nominally the same, we measured the highest  
307 amount of particulate peroxide with 2-butanone peroxide (16.7%), followed by cumene  
308 hydroperoxide (12.7%) and then tert-butyl hydroperoxide (3.8%) using the offline iodometric  
309 method. This trend in particulate peroxide content is consistent with the vapour pressures  
310 calculated using the SIMPOL group contribution method (Pankow et al., 2008), with 2-butanone  
311 peroxide being the least volatile, and tert-butyl hydroperoxide being the most volatile. Also, the  
312 order of particle-phase peroxide content is consistent with the order of  $\gamma_{SO_2}$  observed, as shown in  
313 Fig. 2. A simple visualization of these relationships between different peroxide characteristics  
314 (number of peroxide groups, vapour pressure and aqueous-phase rate constants) and measured  
315  $\gamma_{SO_2}$  (at RH = 50%) is illustrated in Fig. S7, which indicates higher  $\gamma_{SO_2}$  can be expected for  
316 organic peroxides with multiple O-O groups, lower vapour pressures and higher aqueous phase  
317 reactivities. It should be noted that the order of magnitude difference in experimentally measured  
318  $\gamma_{SO_2}$  among various organic peroxides (Fig.2) is still not fully explained when both volatility and  
319 reaction kinetics are taken into account (Fig.S7), suggesting that the reactive uptake may be  
320 influenced by other factors. In summary, for our current experiments where we nominally

321 maintained total injected amount of organic peroxide constant, measured  $\gamma_{\text{SO}_2}$  depends both on  
322 reactivity and gas-particle partitioning of the organic peroxides.

323

### 324 **3.3 SO<sub>2</sub> uptake and aqueous phase kinetics**

325 Since the aqueous phase reaction rate constants between S(IV) and these model organic  
326 peroxides have been measured previously (Wang et al., 2019), we can test our understanding of  
327 the measured  $\gamma_{\text{SO}_2}$  using a simple model. By assuming the amount of SO<sub>2</sub> dissolved in the aerosol  
328 is in equilibrium with the gas phase, the overall  $\gamma_{\text{SO}_2}$  can be expressed using the simplified  
329 resistor model (Hanson et al., 1994):

330

$$331 \frac{1}{\gamma} = \frac{1}{\alpha} + \frac{\bar{c}}{4HRT\sqrt{k^l D_l}} \frac{1}{\left[\coth(q) - \frac{1}{q}\right]} \quad (3)$$

332 where  $\alpha$  is the mass accommodation coefficient,  $\bar{c}$  is the mean molecular speed of SO<sub>2</sub> (cm s<sup>-1</sup>),  
333 H is the effective Henry's law constant that includes both the dissolution of SO<sub>2</sub> and the  
334 dissociation of H<sub>2</sub>SO<sub>3</sub> (M atm<sup>-1</sup>), R is the ideal gas constant (atm L mol<sup>-1</sup> K<sup>-1</sup>), T is the  
335 temperature (K), and the parameter q is used to describe the competition between the reaction  
336 and diffusion of the dissolved gaseous species within a particle, which is further calculated as:

$$337 q = r \sqrt{\frac{k^l}{D_l}} \quad (4)$$

338 where r is the radius (cm) of a given particle,  $D_l$  is the aqueous-phase diffusion coefficient (cm<sup>2</sup>  
339 s<sup>-1</sup>),  $k^l$  is the first order rate constant (s<sup>-1</sup>) for the reaction. For experiments in the current study,  
340 the calculated q values were consistently found to be far less than 1, which indicates a volume-  
341 limited reaction regime. Combining with the assumption of a relatively fast mass  
342 accommodation process compared with the bulk phase reaction, equation (3) can be further  
343 simplified as to describes reactive uptake in the volume-limited regime:

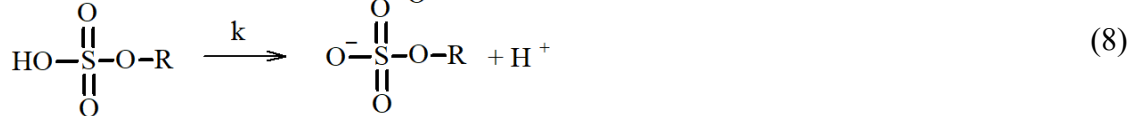
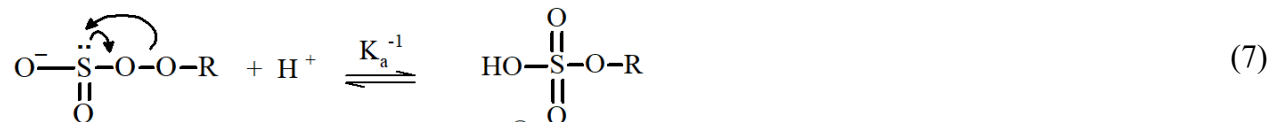
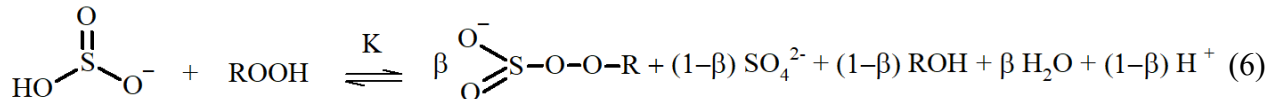
344

$$\gamma = \frac{4HRT[\text{peroxide}]k^{\text{II}} V}{\bar{c} S} \quad (5)$$

345 Here, we assume all the peroxides remain in the condensed phase upon atomizing and reaction  
 346 inside the chamber for the upper-bound prediction of  $\gamma_{\text{SO}_2}$ . [peroxide] represents the particle phase  
 347 concentration of total organic peroxide (M) based on the initial ratio between organic peroxide and  
 348 ammonium sulfate in the atomizing solution, and the aerosol water content output by E-AIM III  
 349 (Clegg et al., 1998),  $k^{\text{II}}$  is the second order reaction rate constant ( $\text{M}^{-1} \text{ s}^{-1}$ ), which we have  
 350 measured in the bulk phase at dilute concentrations previously (Wang et al., 2019), V/S is the ratio  
 351 between particle volume concentration ( $\mu\text{m}^3 \text{ cm}^{-3}$ ) and particle surface area concentration ( $\mu\text{m}^2$   
 352  $\text{cm}^{-3}$ ) derived from SMPS measurements. As a result, the observed reactive uptake coefficient of  
 353  $\text{SO}_2$  can be compared to that predicted from the bulk phase reaction rate constant, and the results  
 354 are shown in Fig. 4 and Fig. S8. Overall, we noticed that this model captures the dependence of  
 355  $\gamma_{\text{SO}_2}$  on peroxide content, but the modeled results were found to be generally 15-50 times lower  
 356 than the experimentally measured values (Fig. S8). The current  $\gamma_{\text{SO}_2}$  predictions are likely upper-  
 357 bound estimates since all the peroxides were assumed to stay in the condensed phase without  
 358 partitioning. As a result, this observed 15-50 times of discrepancy could even be larger if the  
 359 particulate peroxide content during the chamber experiments were lower due to partitioning.  
 360 It should be noted that the calculated  $\gamma_{\text{SO}_2}$  was based on reaction kinetics measured in dilute  
 361 solutions while the experimental  $\gamma_{\text{SO}_2}$  were measured directly from suspended particles. This large  
 362 difference in kinetics between those in aerosol and in dilute bulk solution suggests that this  
 363 multiphase interaction is strongly favored in the highly concentrated aerosol environment. One of  
 364 the potential explanations for this discrepancy could be liquid-liquid phase separation (LLPS) in  
 365 aerosol between organic peroxide and ammonium sulfate (Ciobanu et al., 2009; O'Brien et al.,  
 366 2015) such that  $\text{SO}_2$  can directly interact with the acidic organic phase, where the concentration of

367 peroxides can be higher and the kinetics can be different from what we have measured in dilute  
368 solution (Wang et al., 2019). However, LLPS is generally governed by the chemical composition  
369 of the hydrophobic phase (Freedman, 2017). A higher level of oxygenation in organic aerosol is  
370 related with higher hydrophilicity, which would favor a homogeneous particle instead of phase  
371 separation. Previous studies showed that LLPS did not occur for organic coating with O:C above  
372 0.8 (You et al., 2013; You et al., 2014). The LLPS phenomenon in simple organic–inorganic  
373 mixtures can also be affected by the functional groups. The maximum O:C for LLPS could be 0.71  
374 for organics with multiple carboxylic and hydroxyl groups but low aromatic content (Song et al.,  
375 2012) while the 2-butanone peroxide we used for both  $\gamma_{\text{SO}_2}$  measurement and prediction in the  
376 present study has multiple peroxide groups with an O:C value of 0.75. Particle size could also have  
377 impacts on phase separation (Cheng et al., 2015). Particle diameters in the current study are mainly  
378 under 200 nm while a previous study showed particles smaller than this size are less likely to  
379 experience LLPS (Veghte et al., 2013). We therefore believe that LLPS is not likely to be  
380 responsible for the enhanced uptake rate observed under these experimental conditions.  
381 Another explanation is the high solute strength in the concentrated aerosol phase. Although the  
382 aerosol water content for ammonium sulfate aerosol was found to be higher than that of malonic  
383 acid aerosol under RH 50%. As indicated in Fig. 4 and Fig. S8, the difference between the  
384 measured and predicted  $\gamma_{\text{SO}_2}$  is larger for ammonium sulfate aerosol than for malonic acid.  
385 Meanwhile, the calculated ionic strength in aerosol liquid phase under RH 50% for ammonium  
386 sulfate ( $40 \text{ mol kg}^{-1}$ ) is significantly larger than that of malonic acid ( $0.45 \text{ mol kg}^{-1}$ ). It has been  
387 previously reported that the reaction rate between sulfite and hydrogen peroxide in aqueous phase  
388 increases with ionic strength (Maaß et al., 1999). Based on the reaction mechanisms proposed for

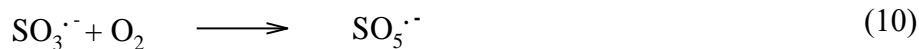
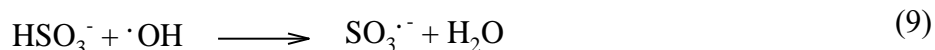
389 dissolved  $\text{SO}_2$  and hydrogen peroxide (Halperin and Taube, 1952), we speculate the reaction  
 390 between aqueous phase S(IV) and organic peroxides to follow a similar mechanism:



391  
 392 where the overall rate constant is equal to  $k \frac{K}{K_a}$ , assuming fast equilibrium steps for reactions 6 and  
 393 7. Dissociated solutes are surrounded by an extended solvation shell which could affect the  
 394 reaction rates (Herrmann, 2003). Fewer available free water molecules would therefore shift the  
 395 equilibrium to the right in equation (6). Additionally, higher ionic strength also corresponds to an  
 396 increased concentration of electrolytes in the aqueous phase, which could hinder the dissociation  
 397 of the peroxymonosulfurous acid and shift the equilibrium in equation (7) to the right. In recent  
 398 work by Liu et al. (2020), the rate of S(IV) oxidation by  $\text{H}_2\text{O}_2$  can be enhanced by up to a factor  
 399 of 50 in aerosol aqueous phase compared to that of dilute solution. The highest ionic strength at  
 400 which such enhancement was measured for the  $\text{H}_2\text{O}_2$  oxidation pathway was  $15 \text{ mol kg}^{-1}$  (Liu et  
 401 al., 2020).

402 Whereas the above analysis is based on the assumption that all the chemistry occurs in the bulk  
 403 component of the particle, it is also possible that some component of the reaction occurs at the gas-  
 404 particle interface and the overall kinetics can be affected by interfacial characteristics. For example,  
 405 an enhanced ionic strength in the aerosol phase can also impact the interfacial reaction mechanisms.  
 406 Previous study has shown evidence that interfacial chemistry is important for  $\text{SO}_2$  oxidation in the

407 aerosol phase (Laskin et al., 2003). With higher ionic strength, anions partitioning to the air-liquid  
 408 interface can promote the overall reaction kinetics via proton transfer and thus accelerate the  
 409 interfacial chemistry (Knipping et al., 2000; Mishra et al., 2012; Mekic et al., 2018; Mekic et al.,  
 410 2020; Wei et al., 2018; Ruiz-Lopez et al., 2020). In addition to the catalytic effects of protons  
 411 indicated in Eqn. 6-8, Hung et al. (2015, 2018) observed significant  $\text{SO}_3^{\cdot-}$  signal at the acidic  
 412 microdroplet surface, which can promote sulfate formation via radical propagation chain initiated  
 413 by surrounding radicals and molecular oxygen (Eqn. 9-12):



414  
 415 where the hydroxy radical can potentially be produced from decomposition of the labile organic  
 416 peroxide in our system (Tong et al., 2016). However, we cannot distinguish whether the interfacial  
 417 protons promote sulfate formation by catalyze the peroxide S(IV) oxidation pathway or the sulfur  
 418 radical pathway at the current stage. In the recent study by Wei et al. (2018), a pH gradient was  
 419 observed for phosphate-buffered aerosol droplets with the proton accumulated at the interface.  
 420 Base on the pH-dependent aqueous phase kinetics measured in our previous work (Wang et al.,  
 421 2019), such interfacial proton accumulation could potentially explain the enhanced kinetics we  
 422 observed for aerosol in the current study. However, the chemical compositions are quite different.  
 423 While phosphate-buffered particles were studied in Wei et al. (2018), acidic ammonium sulfate  
 424 aerosol was used in our study. Also, the particle size in Wei et al. (2018) is significantly larger (20  
 425  $\mu\text{m}$ ) than what was studied in the current study (200 nm). Thus, it should be noted that there is no

426 direct evidence from the current study showing the relationship between the interfacial properties  
427 and  $\gamma_{SO_2}$ , and future studies are warranted.

428 Therefore, while more studies are needed to clearly delineate the roles of ionic strength, interfacial  
429 activity, bulk reactivity, and particle phase state quantitatively, the enhancement of  $SO_2$  oxidation  
430 kinetics by highly concentrated aerosol particles compared to dilute aqueous solutions are  
431 concluded to be large (factor of 15-50) for the experimental conditions in the current study.

432

### 433 **3.4 $SO_2$ uptake and aerosol pH**

434 As indicated by the proposed reaction mechanisms (Eqn. 6-8), protons are important reaction  
435 intermediates for this  $SO_2$  oxidation pathway. Previously, the aqueous phase reaction rate  
436 constants between organic peroxides and dissolved  $SO_2$  were measured to be pH dependent  
437 (Wang et al., 2019). Moreover, the dissolution equilibrium of  $SO_2$  into aqueous phase is also pH  
438 sensitive (Seinfeld and Pandis, 2012). Besides, many studies have shown that the uptake kinetics  
439 for gaseous species can be affected by the condensed phase pH (Shi et al., 1999;Gaston et al.,  
440 2014;Drozd et al., 2013;Jang and Kamens, 2001;Liu et al., 2015). Reactive uptake of ammonia  
441 was observed to depend on condensed phase acidity (Shi et al., 1999). Heterogeneous  
442 condensation of isoprene-derived epoxydiol onto seed aerosol was found to increase with proton  
443 concentration (Gaston et al., 2014). In the current study, the potential impact from particle phase  
444 pH on  $\gamma_{SO_2}$  was explored by adding HCl into the atomizing solution. To estimate the particle  
445 phase pH, two different methods associated with two different assumptions were used. In the  
446 first scenario, the aerosol pH in each experiment was estimated using the E-AIM III model  
447 (Clegg et al., 1998) based on the initial molar ratios of inorganic species ( $H^+$ ,  $NH_4^+$ ,  $SO_4^{2-}$ ,  $Cl^-$ ) in  
448 the atomizing solution and measured RH (around 50%). In the second scenario, the additional

449 sulfate formed from reactive uptake of  $\text{SO}_2$  was taken into consideration. The partitioning of  $\text{HCl}$   
450 was allowed in the model simulation for both scenarios. The formation of sulfate would enhance  
451 the proton concentration in the aerosol liquid phase thus lower the aerosol pH. The average pH  
452 during the  $\text{SO}_2$  uptake process is likely in between these two extremes.

453 Fig. 5 shows the measured reactive uptake coefficients of  $\text{SO}_2$  as a function of the calculated pH.  
454 The reactive uptake coefficient was found to weakly increase with decreasing pH, which is  
455 consistent with acid-catalyzed reactions between peroxides and dissolved  $\text{SO}_2$  as measured in the  
456 bulk phase (Lind et al., 1987; Wang et al., 2019).  $\gamma_{\text{SO}_2}$  was also predicted for the same range of  
457 pH based on Eqn. 5 and the pH-dependent bulk-phase reaction rate constants measured  
458 previously (Wang et al., 2019). Indicated by Fig. 5, the measured  $\gamma_{\text{SO}_2}$  again exceeds the  
459 predicted  $\gamma_{\text{SO}_2}$  by about a factor of 50, which is consistent with what we reported earlier and is  
460 likely due to the effects of aerosol ionic strength.

461 Unlike the observed  $\gamma_{\text{SO}_2}$ , however, the predicted  $\gamma_{\text{SO}_2}$  does not exhibit a monotonic trend.  $\gamma_{\text{SO}_2}$  is  
462 expected to decrease with decreasing pH at high pH ( $>2$ ) as the effective Henry's law constant of  
463  $\text{SO}_2$  decreases with higher acidity (Seinfeld and Pandis, 2012).  $\gamma_{\text{SO}_2}$  is not expected to increase  
464 with decreasing pH until pH is below 2 where the acidity enhancement in reaction rate constant  
465 exceeds the decrease in  $\text{SO}_2$  solubility. As illustrated earlier, extrapolating dilute aqueous-phase  
466 kinetics to the highly concentrated aerosol requires considering effects from high solute strength.  
467 Solute strength may change the pH dependence of  $\gamma_{\text{SO}_2}$  in two ways. First, the solubility of  $\text{SO}_2$   
468 may decrease and become less dependent on pH as ionic strength increases (Rodríguez-Sevilla et  
469 al., 2002). A former study (Leng et al., 2015) has shown that the effective Henry's law of  
470 triethylamine decreases with increased ionic strength. Another potential explanation is that the  
471 aqueous phase reaction rate constant can be more pH-dependent at high ionic strengths than what

472 we measured previously in dilute solutions. In either case, the inflection of the predicted  $\gamma_{\text{SO}_2}$   
473 would change and  $\gamma_{\text{SO}_2}$  could become more negatively dependent on pH ( $d[\gamma_{\text{SO}_2}]/d[\text{pH}]$  becomes  
474 less positive in the high pH range and/or more negative in the low pH range), which would  
475 match more closely with the observed dependence. It should also be noted that there are  
476 substantial uncertainties in estimating pH values, originating from the partitioning of organics,  
477 organic-inorganic phase separations, mixing state of specific ions, uncertain activity coefficients  
478 and the propagation of RH uncertainties (Clegg et al., 2008; Fountoukis et al., 2009; Guo et al.,  
479 2016). Also, the reactive uptake is a dynamic process and will influence aerosol pH in turn upon  
480 sulfate formation. In summary, while the magnitude of predicted  $\gamma_{\text{SO}_2}$  is consistent with our  
481 expected values (after accounting for the enhancement by high aerosol solute strength), we  
482 cannot fully explain the dependence of  $\gamma_{\text{SO}_2}$  on aerosol pH at the current stage. Future studies  
483 should investigate how the effective Henry's law of  $\text{SO}_2$  and pH dependence of reaction rate  
484 constants vary in aerosol liquid phase with high solute strength in order to have a more  
485 comprehensive understanding of the relationship between  $\gamma_{\text{SO}_2}$  and aerosol pH.

#### 486 **3.4 $\text{SO}_2$ uptake onto SOA**

487  $\gamma_{\text{SO}_2}$  was measured for a few model SOA systems, as organic peroxides are abundant in SOA  
488 (Surratt et al., 2006; Kautzman et al., 2009; Krapf et al., 2016; Bonn et al., 2004). Here we studied  
489 SOA formed from monoterpene ozonolysis and toluene photooxidation. It should be noted that  
490 for the  $\gamma_{\text{SO}_2}$  measurements of toluene SOA, a strong hydrocarbon interference was observed with  
491 the  $\text{SO}_2$  analyzer, likely stemming from the high concentrations of gas-phase aromatic  
492 compounds. A rough estimate of the uptake rate for toluene SOA from aerosol mass  
493 spectrometer sulfate measurements is provided in the SI (Section 1). The reactive uptake  
494 coefficient of  $\text{SO}_2$  onto Saharan mineral dust was reported on the order of  $10^{-5}$  (Adams et al.,

495  $\gamma_{\text{SO}_2}$  onto dust with the coexistence of  $\text{NO}_2$  and  $\text{NH}_3$  under various RH conditions were  
496 measured to be  $10^{-7}$  to  $10^{-5}$  (Zhang et al., 2019). For a variety of metal oxides,  $\text{SO}_2$  reactive  
497 uptake coefficients were quantified to be between  $10^{-6}$  and  $10^{-4}$  (Usher et al., 2002; Fu et al.,  
498 2007; Shang et al., 2010). More recently,  $\gamma_{\text{SO}_2}$  studied for heterogeneous sulfate formation by  
499 photolysis of particulate nitrate were reported in the range of  $10^{-6}$  to  $10^{-5}$  (Gen et al., 2019). As  
500 shown in Fig. 6,  $\gamma_{\text{SO}_2}$  for all SOA systems were measured to be on the order of  $10^{-4}$ . Similar  $\gamma_{\text{SO}_2}$   
501 values on the order of  $10^{-4}$  were measured for  $\alpha$ -pinene SOA by Yao et al. (2019), and  $10^{-5}$  for  
502 limonene SOA estimated from the chamber study by Ye et al. (2018). The reaction products  
503 from this SOA and  $\text{SO}_2$  interaction will be reported in a separate study.

504

#### 505 **4. Atmospheric Implications**

506 Oxidation of atmospheric hydrocarbons produces reactive intermediates that can potentially  
507 interact with  $\text{SO}_2$  and form particulate sulfate, contributing to PM formation and growth (Berndt  
508 et al., 2015; Mauldin et al., 2012; Yao et al., 2019). Organic peroxides generated from both  
509 biogenic and anthropogenic hydrocarbon emissions are abundant in submicron aerosol. Given  
510 that they are highly reactive with relatively short lifetimes (Bonn et al., 2004; Krapf et al.,  
511 2016; Qiu et al., 2020), these species could serve as important condensed phase oxidants for gas  
512 phase  $\text{SO}_2$ . Combining laboratory measurements and model predictions, the current study  
513 investigated heterogeneous reactions between  $\text{SO}_2$  and particulate organic peroxide. The  
514 measured  $\gamma_{\text{SO}_2}$  for organic peroxide containing aerosol ranges from  $10^{-5}$  to  $10^{-2}$  in this study.  
515 Based on the modeling work by Wang et al. (2014), adding an  $\text{SO}_2$  uptake pathway to GEOS-  
516 Chem with a reactive uptake coefficient of  $10^{-4}$  could improve the surface sulfate prediction by  
517 more than 50% during a severe haze episode over North China (RH 50%), suggesting the

518 potential importance of this multiphase reaction pathway, especially when SOA is the dominant  
519 component in particulate matter.

520 The dependence of the heterogeneous kinetics on RH, aerosol pH, peroxide type, and peroxide  
521 content were also evaluated. The experimentally measured  $\gamma_{SO_2}$  was found to be consistently  
522 higher than that predicted from reaction kinetics with organic peroxides in the dilute aqueous  
523 phase. This discrepancy can be potentially explained by the effects of high ionic strength  
524 presented in the aerosol, suggesting that the impact from highly concentrated solutes needs to be  
525 taken into consideration when applying aqueous phase kinetics to aerosol multiphase chemistry,  
526 especially for particles containing strong electrolytes. We also observed that the kinetics of this  
527 multiphase reaction exhibit a weak dependence on pH. Increasing the condensed-phase acidity  
528 may enhance the heterogeneous rate constant at low pH, and while this pH dependence is  
529 consistent with that of the aqueous phase reaction rate constant measured previously, it is not  
530 consistent with the decrease of effective Henry's law constant of  $SO_2$  along with enhanced  
531 acidity. Also, it is likely that within the uncertainties, there may not be an observable  $\gamma_{SO_2}$ -pH  
532 trend. Currently, we are not able to fully explain the pH dependence, and further studies are  
533 warranted. Particle phase peroxide content was observed to be linearly correlated with  $\gamma_{SO_2}$ .  
534 Moreover,  $\gamma_{SO_2}$  measured for 2-butanone peroxide was found to be orders of magnitude higher  
535 than that of cumene hydroperoxide and tert-butyl hydroperoxide. The difference in  $\gamma_{SO_2}$  among  
536 various types of organic peroxides can be partially explained by their condensed-phase reactivity  
537 and gas-particle partitioning.

538 In general, we found the observed  $\gamma_{SO_2}$  in this study can be summarized using the following  
539 semiempirical multilinear relationship:

540 
$$\log \gamma = -1.7 + 0.0024 \times k^H + 0.46 \times PAS + 0.024 \times RH - 1.9 \times Vp \quad (13)$$

541 where  $\gamma$  is the reactive uptake coefficient,  $k''$  is the aqueous phase S(IV) oxidation rate constant  
542 ( $M^{-1} s^{-1}$ ),  $PAS$  is the molar ratio between particulate peroxide and ammonium sulfate in the  
543 atomizing solution, which is a proxy for the amount of peroxide in both gas and particle phases  
544 applied in the current study,  $RH$  is the relative humidity (%),  $Vp$  is the vapour pressure (kPa) of  
545 the peroxide. Fig. 7 illustrates the degree to which this semi-empirical expression describes the  
546 experimental data for ammonium sulfate aerosol mixed with the three types of organic peroxides.  
547 Residual evaluations of this multilinear regression can be found Fig. S9. We caution that this  
548 equation is not directly applicable to atmospheric models in its current form, especially since the  
549 particle phase peroxide content (PAS) value we applied as input is a calculated value, rather than  
550 a measurement. However, it illustrates the internal consistency of our experimental results across  
551 a range of RH, peroxide content, and aqueous phase reactivities, which are the key variables for  
552 uptake rates. Better understanding of ionic strengths and pH in aerosol, either through modeling  
553 or direct measurements of these variables, is needed to establish the coefficient dependence.  
554 Future studies should be focused on exploring  $\gamma_{SO_2}$  and the reaction products for various types of  
555 SOA as well as ambient particles under atmospherically relevant conditions, evaluating the  
556 underlying impacts from photochemical condition, chemical composition, particle morphology,  
557 ionic strength and interfacial properties on this multiphase physicochemical process. Overall,  
558  $\gamma_{SO_2}$  presented in our study and its relationship with ambient RH, aerosol pH, ionic strength,  
559 particulate peroxide content and type could provide a framework for the implementation of this  
560 heterogeneous mechanism in atmospheric models to have a better understanding of ambient  
561 sulfate formation and particle growth.  
562  
563

564 *Author contributions*

565 A.W.H. C. and S.W. designed the study. S.W., T. L., and J. J. performed the experiments. S.W.,  
566 A.W.H. C., T. L., and J. J. analyzed data. S.W. and A.W.H. C. wrote the manuscript with the  
567 input from all co-authors.

568

569 *Data availability*

570 All data presented in this study are available in the supplemental material and have been  
571 deposited in figshare.

572

573 *Associated content*

574 Supporting Information.

575

576 *Competing interests*

577 The authors declare no competing financial interest.

578

579 *Acknowledgements*

580 This work was supported by Natural Sciences and Engineering Research Council Discovery Grant.  
581 The authors would like to thank Dr. Greg Evans, Dr. Yue Zhao and Dr. Christopher Lim for helpful  
582 comments and discussions. Special thanks to SOCAAR for providing the SO<sub>2</sub> analyzer.

583

584

585

586

587

588 **Reference**

589 Abbatt, J. P. D., Lee, A. K. Y., and Thornton, J. A.: Quantifying trace gas uptake to tropospheric  
590 aerosol: recent advances and remaining challenges, *Chem. Soc. Rev.*, 41, 6555–6581,  
591 <https://doi.org/10.1039/c2cs35052a>, 2012.

592 Adams, J. W., Rodriguez, D., and Cox, R. A.: The uptake of SO<sub>2</sub> on Saharan dust: a flow tube  
593 study, *Atmos. Chem. Phys.*, 5, 2643–2676, doi:10.5194/acp-5-2643-2005, 2005.

594 Andreae, M.O., Afchine, A., Albrecht, R., Holanda, B.A., Artaxo, P., Barbosa, H.M., Borrmann,  
595 S., Cecchini, M.A., Costa, A., Dollner, M. and Fütterer, D.: Aerosol characteristics and particle  
596 production in the upper troposphere over the Amazon Basin, *Atmos. Chem. Phys.*, 18, 921–961,  
597 2018.

598 Atkinson, R., and Arey, J.: Atmospheric degradation of volatile organic compounds, *Chem.*  
599 *Rev.*, 103, 4605–4638, 2003.

600 Berndt, T., Richters, S., Kaethner, R., Voigtländer, J., Stratmann, F., Sipilä, M., Kulmala, M.,  
601 and Herrmann, H.: Gas-phase ozonolysis of cycloalkenes: Formation of highly oxidized RO<sub>2</sub>  
602 radicals and their reactions with NO, NO<sub>2</sub>, SO<sub>2</sub>, and other RO<sub>2</sub> radicals, *J. Phys. Chem. A*, 119,  
603 10336–10348, 10.1021/acs.jpca.5b07295, 2015.

604 Bianchi, F., Kurtén, T., Riva, M., Mohr, C., Rissanen, M. P., Roldin, P., Berndt, T., Crounse, J.  
605 D., Wennberg, P. O., Mentel, T. F., Wildt, J., Junninen, H., Jokinen, T., Kulmala, M., Worsnop,  
606 D. R., Thornton, J. A., Donahue, N., Kjaergaard, H. G., and Ehn, M.: Highly oxygenated organic  
607 molecules (HOM) from gas-phase autoxidation involving peroxy radicals: A key contributor to  
608 atmospheric aerosol, *Chem. Rev.*, 119, 3472–3509, 10.1021/acs.chemrev.8b00395, 2019.

609 Bonn, B., von Kuhlmann, R., and Lawrence, M. G.: High contribution of biogenic  
610 hydroperoxides to secondary organic aerosol formation, *Geophys. Res. Lett.*, 31, L10108,  
611 <https://doi.org/10.1029/2003GL019172>, 2004.

612 Chen, Q., Farmer, D. K., Schneider, J., Zorn, S. R., Heald, C. L., Karl, T. G., Guenther, A.,  
613 Allan, J. D., Robinson, N., Coe, H., Kimmel, J. R., Pauliquevis, T., Borrmann, S., Pöschl, U.,  
614 Andreae, M. O., Artaxo, P., Jimenez, J. L., and Martin, S. T.: Mass spectral characterization of  
615 submicron biogenic organic particles in the Amazon Basin, *Geophys. Res. Lett.*, 36, L20806,  
616 <https://doi.org/10.1029/2009GL039880>, 2009.

617 Chen, T., Chu, B., Ge, Y., Zhang, S., Ma, Q., He, H., and Li, S.-M.: Enhancement of aqueous  
618 sulfate formation by the coexistence of NO<sub>2</sub>/NH<sub>3</sub> under high ionic strengths in aerosol water,  
619 *Environ. Pollut.*, 252, 236–244, <https://doi.org/10.1016/j.envpol.2019.05.119>, 2019.

620 Cheng, Y., Su, H., Koop, T., Mikhailov, E., and Pöschl, U.: Size dependence of phase transitions  
621 in aerosol nanoparticles, *Nat. Commun.*, 6, 5923, 10.1038/ncomms6923, 2015.

622 Cheng, Y. F., Zheng, G. J., Wei, C., Mu, Q., Zheng, B., Wang, Z. B., Gao, M., Zhang, Q., He, K.  
623 B., Carmichael, G., Pöschl, U., and Su, H.: Reactive nitrogen chemistry in aerosol water as a  
624 source of sulfate during haze events in China, *Sci. Adv.*, 2, e1601530, 2016.

625 Ciobanu, V. G., Marcolli, C., Krieger, U. K., Weers, U., and Peter, T.: Liquid-liquid phase  
626 separation in mixed organic/inorganic aerosol particles, *J. Phys. Chem. A*, 113, 10966–10978,  
627 2009.

628 Clegg, S. L., Brimblecombe, P., and Wexler, A. S.: Thermodynamic model of the system  
629  $\text{H}^+ - \text{NH}_4^+ - \text{Na}^+ - \text{SO}_4^{2-} - \text{NO}_3^- - \text{Cl}^- - \text{H}_2\text{O}$  at 298.15 K, *J. Phys. Chem. A*, 102, 2155–2171,  
630 <https://doi.org/10.1021/jp973043j>, 1998.

631 Clegg, S. L., Kleeman, M. J., Griffin, R. J., and Seinfeld, J. H.: Effects of uncertainties in the  
632 thermodynamic properties of aerosol components in an air quality model – Part 1: Treatment of  
633 inorganic electrolytes and organic compounds in the condensed phase, *Atmos. Chem. Phys.*, 8,  
634 1057–1085, <http://www.atmos-chem-phys.net/8/1057/2008/>, 2008.

635 Ding, J., Zhao, P., Su, J., Dong, Q., Du, X., and Zhang, Y.: Aerosol pH and its driving factors in  
636 Beijing, *Atmos. Chem. Phys.*, 19, 7939-7954, 10.5194/acp-19-7939-2019, 2019.

637 Docherty, K. S., Wu, W., Lim, Y. B., and Ziemann, P. J.: Contributions of organic peroxides to  
638 secondary aerosol formed from reactions of monoterpenes with  $\text{O}_3$ , *Environ. Sci. Technol.*, 39,  
639 4049-4059, 2005.

640 Dovrou, E., Rivera-Rios, J. C., Bates, K. H., and Keutsch, F. N.: Sulfate formation via cloud  
641 processing from isoprene hydroxyl hydroperoxides (ISOPPOOH), *Environ. Sci. Technol.*, 53,  
642 12476-12484, 10.1021/acs.est.9b04645, 2019.

643 Drozd, G. T., Woo, J. L., and McNeill, V. F.: Self-limited uptake of  $\alpha$ -pinene oxide to acidic  
644 aerosol: the effects of liquid-liquid phase separation and implications for the formation of  
645 secondary organic aerosol and organosulfates from epoxides, *Atmos. Chem. Phys.*, 13, 8255–  
646 8263, doi:10.5194/acp-13-8255-2013, 2013.

647 Epstein, S. A., Blair, S. L., and Nizkorodov, S. A.: Direct photolysis of  $\alpha$ -pinene ozonolysis  
648 secondary organic aerosol: effect on particle mass and peroxide content, *Environ. Sci. Technol.*,  
649 48, 11251-11258, 2014.

650 Fairlie, T. D., Jacob, D. J., Dibb, J. E., Alexander, B., Avery, M. A., van Donkelaar, A., and  
651 Zhang, L.: Impact of mineral dust on nitrate, sulfate, and ozone in transpacific Asian pollution  
652 plumes, *Atmos. Chem. Phys.*, 10, 3999–4012, doi:10.5194/acp-10-3999-2010, 2010.

653 Fountoukis, C., Nenes, A., Sullivan, A., Weber, R., Van Reken, T., Fischer, M., Matas, E.,  
654 Moya, M., Farmer, D., and Cohen, R. C.: Thermodynamic characterization of Mexico City  
655 aerosol during MILAGRO 2006, *Atmos. Chem. Phys.*, 9, 2141–2156, 2009.

656 Freedman, M. A.: Phase separation in organic aerosol, *Chem. Soc. Rev.*, 46, 7694–7705,  
657 <https://doi.org/10.1039/C6CS00783J>, 2017.

658 Fu, H. B., Wang, X., Wu, H. B., Yin, Y., and Chen, J. M.: Heterogeneous uptake and oxidation  
659 of  $\text{SO}_2$  on iron oxides, *J. Phys. Chem. C*, 111, 6077–6085, 2007.

660 Gao, M., Carmichael, G. R., Wang, Y., Saide, P. E., Yu, M., Xin, J., Liu, Z., and Wang, Z.:  
661 Modeling study of the 2010 regional haze event in the North China Plain, *Atmos. Chem. Phys.*,  
662 16, 1673–1691, <https://doi.org/10.5194/acp-16-1673-2016>, 2016.

663 Gaston, C. J., Riedel, T. P., Zhang, Z., Gold, A., Surratt, J. D., and Thornton, J. A.: Reactive  
664 uptake of an isoprene-derived epoxydiol to submicron aerosol particles, *Environ. Sci. Technol.*,  
665 48, 11178-11186, 10.1021/es5034266, 2014.

666 Gen, M., Zhang, R., Huang, D. D., Li, Y., and Chan, C. K.: Heterogeneous  $\text{SO}_2$  oxidation in  
667 sulfate formation by photolysis of particulate nitrate, *Environ. Sci. Tech. Lett.*, 6, 86–91,  
668 <https://doi.org/10.1021/acs.estlett.8b00681>, 2019.

669 Griffiths, P. T., Badger, C. L., Cox, R. A., Folkers, M., Henk, H. H., and Mentel, T. F.: Reactive  
670 uptake of  $\text{N}_2\text{O}_5$  by aerosols containing dicarboxylic acids. Effect of particle phase, composition,  
671 and nitrate content, *J. Phys. Chem. A*, 113, 5082–5090, 10.1021/jp8096814, 2009.

672 Gunz, D. W. and Hoffmann, M. R.: Atmospheric chemistry of peroxides: A review, *Atmos.*  
673 *Environ.*, 24A, 1601–1633, [https://doi.org/10.1016/0960-1686\(90\)90496-A](https://doi.org/10.1016/0960-1686(90)90496-A), 1990.

674 Guo, H., Sullivan, A. P., Campuzano-Jost, P., Schroder, J. C., LopezHilfiker, F. D., Dibb, J. E.,  
675 Jimenez, J. L., Thornton, J. A., Brown, S. S., Nenes, A., and Weber, R. J.: Fine particle pH and  
676 the partitioning of nitric acid during winter in the northeastern United States, *J. Geophys. Res.*  
677 *Atmos.*, 121, 10355–10376, <https://doi.org/10.1002/2016JD025311>, 2016.

678 Guo, H., Weber, R. J., and Nenes, A.: High levels of ammonia do not raise fine particle pH  
679 sufficiently to yield nitrogen oxide-dominated sulfate production, *Sci. Rep.*, 7, 12109, 2017.

680 Hallquist, M., Wenger, J. C., Baltensperger, U., Rudich, Y., Simpson, D., Claeys, M., Dommen,  
681 J., Donahue, N. M., George, C., Goldstein, A. H., Hamilton, J. F., Herrmann, H., Hoffmann, T.,  
682 Iinuma, Y., Jang, M., Jenkin, M. E., Jimenez, J. L., Kiendler-Scharr, A., Maenhaut, W.,  
683 McFiggans, G., Mentel, Th. F., Monod, A., Prévôt, A. S. H., Seinfeld, J. H., Surratt, J. D.,  
684 Szmigielski, R., and Wildt, J.: The formation, properties and impact of secondary organic  
685 aerosol: current and emerging issues, *Atmos. Chem. Phys.*, 9, 5155–5236, 2009.

686 Halperin, J., and Taube, H.: The transfer of oxygen atoms in oxidation—reduction reactions. IV.  
687 The reaction of hydrogen peroxide with sulfite and thiosulfate, and of oxygen, manganese  
688 dioxide and of permanganate with sulfite, *J. Am. Chem. Soc.*, 74, 380–382, 1952.

689 Hanson, D. R., Ravishankara, A. R., and Solomon, S.: Heterogeneous reactions in sulfuric acid  
690 aerosols: A framework for model calculations, *J. Geophys. Res.*, 99, 3615, <https://doi.org/10.1029/93JD02932>, 1994.

692 Hartz, K. E. H., Rosenorn, T., Ferchak, S. R., Raymond, T. M., Bilde, M., Donahue, N. M., and  
693 Pandis, S. N.: Cloud condensation nuclei activation of monoterpene and sesquiterpene  
694 secondary organic aerosol, *J. Geophys. Res.-Atmos.*, 110(D14), D14208, 2005.

695 He, L.-Y., Huang, X.-F., Xue, L., Hu, M., Lin, Y., Zheng, J., Zhang, R., and Zhang, Y.-H.:  
696 Submicron aerosol analysis and organic source apportionment in an urban atmosphere  
697 in Pearl River Delta of China using high-resolution aerosol mass spectrometry, *J. Geophys. Res.*  
698 *Atmos.*, 116, D12304, <https://doi.org/10.1029/2010JD014566>, 2011.

699 Herrmann, H.: Kinetics of aqueous phase reactions relevant for atmospheric chemistry, *Chem.*  
700 *Rev.*, 103, 4691–4716, 2003.

701 Hildebrandt, L., Donahue, N. M., Pandis, S. N.: High formation of secondary organic aerosol  
702 from the photo-oxidation of toluene, *Atmos. Chem. Phys.*, 9, 2973–2986, 2009.

703 Huang, L., An, J., Koo, B., Yarwood, G., Yan, R., Wang, Y., Huang, C., and Li, L.: Sulfate  
704 formation during heavy winter haze events and the potential contribution from heterogeneous  
705  $\text{SO}_2 + \text{NO}_2$  reactions in the Yangtze River Delta region, China, *Atmos. Chem. Phys.*, 19, 14311–  
706 14328, 10.5194/acp-19-14311-2019, 2019.

707 Huang, L., Coddens, E. M., and Grassian, V. H.: Formation of organosulfur compounds from  
708 aqueous phase reactions of S (IV) with methacrolein and methyl vinyl ketone in the presence of  
709 transition metal ions, *ACS Earth Space Chem.*, 3, 1749–1755, 2019.

710 Huang, L., Liu, T. and Grassian, V. H.: Radical-initiated formation of aromatic organosulfates  
711 and sulfonates in the aqueous phase. *Environ. Sci. Technol.*, 54, 11857–11864, 2020.

712 Huang, R. J., Zhang, Y. L., Bozzetti, C., Ho, K. F., Cao, J. J., Han, Y. M., Daellenbach, K. R.,  
713 Slowik, J. G., Platt, S. M., Canonaco, F., Zotter, P., Wolf, R., Pieber, S. M., Bruns, E. A., Crippa,  
714 M., Ciarelli, G., Piazzalunga, A., Schwikowski, M., Abbaszade, G., Schnelle-Kreis, J.,  
715 Zimmermann, R., An, Z., Szidat, S., Baltensperger, U., Haddad, I. E., and Prevot, A. S. H.: High  
716 secondary aerosol contribution to particulate pollution during haze events in China, *Nature*, 514,  
717 218–222, 2014.

718 Huang, R. J., He, Y., Duan, J., Li, Y., Chen, Q., Zheng, Y., Chen, Y., Hu, W., Lin, C., Ni, H.,  
719 Dai, W., Cao, J., Wu, Y., Zhang, R., Xu, W., Ovadnevaite, J., Ceburnis, D., Hoffmann, T., and  
720 O'Dowd, C. D.: Contrasting sources and processes of particulate species in haze days with low  
721 and high relative humidity in wintertime Beijing, *Atmos. Chem. Phys.*, 20, 9101-9114,  
722 10.5194/acp-20-9101-2020, 2020.

723 Hung, H. M. and Hoffmann, M. R.: Oxidation of gas-phase SO<sub>2</sub> on the surfaces of acidic  
724 microdroplets: Implications for sulfate and sulfate radical anion formation in the atmospheric  
725 liquid phase, *Environ. Sci. Technol.*, 49, 13768–13776, 2015.

726 Hung, H. M., Hsu, M. N., and Hoffmann, M. R.: Quantification of SO<sub>2</sub> oxidation on interfacial  
727 surfaces of acidic micro-droplets: Implication for ambient sulfate formation, *Environ. Sci.*  
728 *Technol.*, 52, 9079–9086, <https://doi.org/10.1021/acs.est.8b01391>, 2018.

729 Jang, M., and Kamens, R. M.: Atmospheric secondary aerosol formation by heterogeneous  
730 reactions of aldehydes in the presence of a sulfuric acid aerosol catalyst, *Environ. Sci. Technol.*,  
731 35, 4758-4766, 10.1021/es010790s, 2001.

732 Jimenez, J. L., Canagaratna, M. R., Donahue, N. M., Prevot, A. S. H., Zhang, Q., Kroll, J. H.,  
733 DeCarlo, P. F., Allan, J. D., Coe, H., Ng, N. L., Aiken, A. C., Docherty, K. S., Ulbrich, I. M.,  
734 Grieshop, A. P., Robinson, A. L., Duplissy, J., Smith, J. D., Wilson, K. R., Lanz, V. A., Hueglin,  
735 C., Sun, Y. L., Tian, J., Laaksonen, A., Raatikainen, T., Rautiainen, J., Vaattovaara, P., Ehn, M.,  
736 Kulmala, M., Tomlinson, J. M., Collins, D. R., Cubison, M. J., Dunlea, J., Huffman, J. A.,  
737 Onasch, T. B., Alfarra, M. R., Williams, P. I., Bower, K., Kondo, Y., Schneider, J., Drewnick,  
738 F., Borrmann, S., Weimer, S., Demerjian, K., Salcedo, D., Cottrell, L., Griffin, R., Takami, A.,  
739 Miyoshi, T., Hatakeyama, S., Shimono, A., Sun, J. Y., Zhang, Y. M., Dzepina, K., Kimmel,  
740 J. R., Sueper, D., Jayne, J. T., Herndon, S. C., Trimborn, A. M., Williams, L. R., Wood, E. C.,  
741 Middlebrook, A. M., Kolb, C. E., Baltensperger, U., and Worsnop, D. R.: Evolution of organic  
742 aerosols in the atmosphere, *Science*, 326, 1525–1529, <https://doi.org/10.1126/science.1180353>,  
743 2009.

744 Kautzman, K., Surratt, J., Chan, M., Chan, A., Hersey, S., Chhabra, P., Dalleska, N., Wennberg,  
745 P., Flagan, R., and Seinfeld, J.: Chemical composition of gas-and aerosol-phase products from  
746 the photooxidation of naphthalene, *J. Phys. Chem. A*, 114, 913-934, 2009.

747 Knipping, E. M., Lakin, M. J., Foster, K. L., Jungwirth, P., Tobias, D. J., Gerber, R. B., Dabdub,  
748 D., and Finlayson-Pitts, B. J.: Experiments and simulations of ion-enhanced interfacial chemistry  
749 on aqueous NaCl aerosols, *Science*, 288, 301, 10.1126/science.288.5464.301, 2000.

750 Krapf, M., El Haddad, I., Bruns, E. A., Molteni, U., Daellenbach, K. R., Prévôt, A. S.,  
751 Baltensperger, U., and Dommen, J.: Labile peroxides in secondary organic aerosol, *Chem*, 1,  
752 603-616, 2016.

753 Laskin, A., Gaspar, D. J., Wang, W., Hunt, S. W., Cowin, J. P., Colson, S. D., and Finlayson-  
754 Pitts, B. J.: Reactions at interfaces as a source of sulfate formation in sea-salt particles, *Science*,  
755 301, 340, 10.1126/science.1085374, 2003.

756 Leng, C. B., Roberts, J. E., Zeng, G., Zhang, Y. H., and Liu, Y.: Effects of temperature, pH, and  
757 ionic strength on the Henry's law constant of triethylamine, *Geophys. Res. Lett.*, 42, 3569-3575,  
758 10.1002/2015gl063840, 2015.

759 Li, G., Bei, N., Cao, J., Huang, R., Wu, J., Feng, T., Wang, Y., Liu, S., Zhang, Q., Tie, X., and  
760 Molina, L. T.: A possible pathway for rapid growth of sulfate during haze days in China, *Atmos.*  
761 *Chem. Phys.*, 17, 3301–3316, <https://doi.org/10.5194/acp17-3301-2017>, 2017.

762 Li, J., Zhang, Y.L., Cao, F., Zhang, W., Fan, M., Lee, X., and Michalski, G.: Stable sulfur  
763 isotopes revealed a major role of transition-metal ion-catalyzed SO<sub>2</sub> oxidation in haze episodes,  
764 *Environ. Sci. Technol.*, 54, 2626–2634, <https://doi.org/10.1021/acs.est.9b07150>, 2020.

765 Lind, J. A., Lazrus, A. L., and Kok, G. L.: Aqueous phase oxidation of sulfur (IV) by hydrogen  
766 peroxide, methylhydroperoxide, and peroxyacetic acid, *J. Geophys. Res. Atmos.*, 92, 4171-4177,  
767 1987.

768 Liu, C., Chen, T., Liu, Y., Liu, J., He, H., Zhang, P.: Enhancement of secondary organic aerosol  
769 formation and its oxidation state by SO<sub>2</sub> during photooxidation of 2-methoxyphenol, *Atmos.*  
770 *Chem. Phys.*, 19, 2687-2700, 2019.

771 Liu, L., Bei, N., Wu, J., Liu, S., Zhou, J., Li, X., Yang, Q., Feng, T., Cao, J., Tie, X. and Li, G.:  
772 Effects of stabilized Criegee intermediates (sCIs) on sulfate formation: a sensitivity analysis  
773 during summertime in Beijing–Tianjin–Hebei (BTH), China, *Atmos. Chem. Phys.*, 19, 13341-  
774 13354, 2019.

775 Liu, T., Clegg, S. L. and Abbatt, J. P. D.: Fast oxidation of sulfur dioxide by hydrogen peroxide  
776 in deliquesced aerosol particles, *Proc. Natl. Acad. Sci. U. S. A.*, 117, 1354–1359, 2020.

777 Liu, Y., Liggio, J., Staebler, R., and Li, S. M.: Reactive uptake of ammonia to secondary organic  
778 aerosols: kinetics of organonitrogen formation, *Atmos. Chem. Phys.*, 15, 13569–13584, 2015.

779 Maaß, F., Elias, H., and Wannowius, K. J.: Kinetics of the oxidation of hydrogen sulfite by  
780 hydrogen peroxide in aqueous solution: ionic strength effects and temperature dependence,  
781 *Atmos. Environ.*, 33, 4413-4419, [https://doi.org/10.1016/S1352-2310\(99\)00212-5](https://doi.org/10.1016/S1352-2310(99)00212-5), 1999.

782 Mauldin, R. L., Berndt, T., Sipilä, M., Paasonen, P., Petäjä, T., Kim, S., Kurtén, T., Stratmann,  
783 F., Kerminen, V. M., and Kulmala, M.: A new atmospherically relevant oxidant of sulphur  
784 dioxide, *Nature*, 488, 193–196, <https://doi.org/10.1038/nature11278>, 2012.

785 Mekic, M., Loisel, G., Zhou, W., Jiang, B., Vione, D., and Gligorovski, S.: Ionic-strength effects  
786 on the reactive uptake of ozone on aqueous pyruvic acid: Implications for air–sea ozone  
787 deposition, *Environ. Sci. Technol.*, 52, 12306-12315, 10.1021/acs.est.8b03196, 2018.

788 Mekic, M., Zeng, J., Zhou, W., Loisel, G., Jin, B., Li, X., Vione, D., and Gligorovski, S.: Ionic  
789 strength effect on photochemistry of fluorene and dimethylsulfoxide at the air–sea interface:  
790 Alternative formation pathway of organic sulfur compounds in a marine atmosphere, *ACS Earth*  
791 *Space Chem.*, 4, 1029-1038, 10.1021/acsearthspacechem.0c00059, 2020.

792 Mishra, H., Enami, S., Nielsen, R. J., Hoffmann, M. R., Goddard, W. A., and Colussi, A. J.:  
793 Anions dramatically enhance proton transfer through aqueous interfaces, *Proc. Natl. Acad. Sci.*  
794 U. S. A.

795 Newland, M. J., Rickard, A. R., Vereecken, L., Muñoz, A., Ródenas, M., and Bloss, W. J.:  
796 Atmospheric isoprene ozonolysis: impacts of stabilised Criegee intermediate reactions with SO<sub>2</sub>,  
797 H<sub>2</sub>O and dimethyl sulfide, *Atmos. Chem. Phys.*, 15, 9521–9536, <https://doi.org/10.5194/acp-15-9521-2015>, 2015.

799 Ng, N., Kroll, J., Chan, A., Chhabra, P., Flagan, R., and Seinfeld, J.: Secondary organic aerosol  
800 formation from m-xylene, toluene, and benzene, *Atmos. Chem. Phys.*, 7, 3909–3922,  
801 <http://www.atmos-chem-phys.net/7/3909/2007>, 2007.

802 Ng, N. L., Kwan, A. J., Surratt, J. D., Chan, A. W. H., Chhabra, P. S., Sorooshian, A., Pye, H. O.  
803 T., Crounse, J. D., Wennberg, P. O., Flagan, R. C., and Seinfeld, J. H.: Secondary organic  
804 aerosol (SOA) formation from reaction of isoprene with nitrate radicals (NO<sub>3</sub>), *Atmos. Chem.*  
805 *Phys.*, 8, 4117–4140, <http://www.atmos-chem-phys.net/8/4117/2008/>, 2008.

806 Nguyen, T. B., Tyndall, G. S., Crounse, J. D., Teng, A. P., Bates, K. H., Schwantes, R. H.,  
807 Coggon, M. M., Zhang, L., Feiner, P., Milller, D. O., Skog, K. M., Rivera-Rios, J. C., Dorris, M.,  
808 Olson, K. F., Koss, A., Wild, R. J., Brown, S. S., Goldstein, A. H., de Gouw, J. A., Brune,  
809 W. H., Keutsch, F. N., Seinfeld, J. H., and Wennberg, P. O.: Atmospheric fates of Criegee  
810 intermediates in the ozonolysis of isoprene, *Phys. Chem. Chem. Phys.*, 18, 10 241–10 254,  
811 <https://doi.org/10.1039/C6CP00053C>, <http://dx.doi.org/10.1039/C6CP00053C>, 2016.

812 O'Brien, R. E., Wang, B., Kelly, S. T., Lundt, N., You, Y., Bertram, A. K., Leone, S. R., Laskin,  
813 A., and Gilles, M. K.: Liquid–liquid phase separation in aerosol particles: Imaging at the  
814 nanometer scale, *Environ. Sci. Technol.*, 49, 4995–5002, 10.1021/acs.est.5b00062, 2015.

815 Pankow, J. F. and Asher, W. E.: SIMPOL.1: a simple group contribution method for predicting  
816 vapor pressures and enthalpies of vaporization of multifunctional organic compounds, *Atmos.*  
817 *Chem. Phys.*, 8, 2773–2796, <http://www.atmos-chem-phys.net/8/2773/2008/>, 2008.

818 Qiu, J., Liang, Z., Tonokura, K., Colussi, A. J., and Enami, S.: Stability of monoterpane-derived  
819 α-hydroxyalkyl-hydroperoxides in aqueous organic media – relevance to the fate of  
820 hydroperoxides in aerosol particle phases, *Environ. Sci. Technol.*, 10.1021/acs.est.9b07497,  
821 2020.

822 Rodríguez-Sevilla, J., Álvarez, M., Limiñana, G., Díaz, M. C.: Dilute SO<sub>2</sub> absorption equilibria  
823 in aqueous HCl and NaCl solutions at 298.15 K, *J. Chem. Eng. Data*, 47, 1339–1345, 2002.

824 Ruiz-Lopez, M.F., Francisco, J.S., Martins-Costa, M.T. and Anglada, J.M.: Molecular reactions  
825 at aqueous interfaces. *Nat. Rev. Chem.*, 1–17, 2020.

826 Seinfeld, J. H., and Pandis, S. N.: *Atmospheric chemistry and physics: from air pollution to*  
827 *climate change*, John Wiley & Sons, 2012.

828 Sha, T., Ma, X., Jia, H., Tian, R., Chang, Y., Cao, F., and Zhang, Y.: Aerosol chemical  
829 component: Simulations with WRF-Chem and comparison with observations in Nanjing, *Atmos.*  
830 *Environ.*, 218, 116982, <https://doi.org/10.1016/j.atmosenv.2019.116982>, 2019.

831 Shang, J., Li, J., Zhu, T.: Heterogeneous reaction of SO<sub>2</sub> on TiO<sub>2</sub> particles. *Sci. China Chem.*, 53,  
832 2637–2643, 2010.

833 Shi, G., Xu, J., Peng, X., Xiao, Z., Chen, K., Tian, Y., Guan, X., Feng, Y., Yu, H., Nenes, A.,  
834 and Russell, A. G.: pH of aerosols in a polluted atmosphere: Source contributions to highly  
835 acidic aerosol, *Environ. Sci. Technol.*, 51, 4289-4296, 10.1021/acs.est.6b05736, 2017.

836 Shi, Q., Davidovits, P., Jayne, J. T., Worsnop, D. R., and Kolb, C. E.: Uptake of gas-phase  
837 ammonia. 1. Uptake by aqueous surfaces as a function of pH, *J. Phys. Chem. A*, 103, 8812-8823,  
838 10.1021/jp991696p, 1999.

839 Song, M., Marcolli, C., Krieger, U. K., Zuend, A., and Peter, T.: Liquid–liquid phase separation  
840 in aerosol particles: dependence on O:C, organic functionalities, and compositional complexity,  
841 *Geophys. Res. Lett.*, 39, L19801, doi:10.1029/2012GL052807, 2012.

842 Song, S., Gao, M., Xu, W., Shao, J., Shi, G., Wang, S., Wang, Y., Sun, Y., and McElroy, M. B.:  
843 Fine-particle pH for Beijing winter haze as inferred from different thermodynamic equilibrium  
844 models, *Atmos. Chem. Phys.*, 18, 7423–7438, <https://doi.org/10.5194/acp-18-7423-2018>, 2018.

845 Song, S., Gao, M., Xu, W., Sun, Y., Worsnop, D. R., Jayne, J. T., Zhang, Y., Zhu, L., Li, M.,  
846 Zhou, Z., Cheng, C., Lv, Y., Wang, Y., Peng, W., Xu, X., Lin, N., Wang, Y., Wang, S., Munger,  
847 J. W., Jacob, D. J., and McElroy, M. B.: Possible heterogeneous chemistry of hydroxy  
848 methanesulfonate (HMS) in northern China winter haze, *Atmos. Chem. Phys.*, 19, 1357–1371,  
849 <https://doi.org/10.5194/acp-19-1357-2019>, 2019.

850 Su, H., Cheng, Y., and Pöschl, U.: New multiphase chemical processes influencing atmospheric  
851 aerosols, air quality, and climate in the anthropocene, *Accounts Chem. Res.*, 53, 2034–2043,  
852 <https://doi.org/10.1021/acs.accounts.0c00246>, 2020.

853 Sun, Y., Wang, Z., Fu, P., Jiang, Q., Yang, T., Li, J., and Ge, X.: The impact of relative humidity  
854 on aerosol composition and evolution processes during wintertime in Beijing, China, *Atmos.*  
855 *Environ.*, 77, 927-934, 2013.

856 Surratt, J. D., Murphy, S. M., Kroll, J. H., Ng, N. L., Hildebrandt, L., Sorooshian, A.,  
857 Szmigielski, R., Vermeylen, R., Maenhaut, W., and Claeys, M.: Chemical composition of  
858 secondary organic aerosol formed from the photooxidation of isoprene, *J. Phys. Chem. A*, 110,  
859 9665-9690, 2006.

860 Thornton, J. A., Braban, C. F., and Abbatt, J. P. D.: N<sub>2</sub>O<sub>5</sub> hydrolysis on sub-micron organic  
861 aerosols: the effect of relative humidity, particle phase, and particle size, *Phys. Chem. Chem.*  
862 *Phys.*, 5, 4593–4603, <https://doi.org/10.1039/B307498F>, 2003.

863 Tie, X., Brasseur, G., Emmons, L., Horowitz, I., and Kinnison, D.: Effects of aerosols on  
864 tropospheric oxidants: a global model study, *J. Geophys. Res. Atmos.*, 106, 22931–22964, 2001.

865 Tong, H., Arangio, A. M., Lakey, P. S. J., Berkemeier, T., Liu, F., Kampf, C. J., Brune, W. H.,  
866 Pöschl, U., and Shiraiwa, M.: Hydroxyl radicals from secondary organic aerosol decomposition  
867 in water, *Atmos. Chem. Phys.*, 16, 1761–1771, doi:10.5194/acp-16-1761-2016, 2016.

868 Usher, C. R., Al-Hosney, H., Carlos-Cuellar, S., and Grassian, V. H.: A laboratory study of the  
869 heterogeneous uptake and oxidation of sulfur dioxide on mineral dust particles, *J. Geophys. Res.*,  
870 107, 4713, doi:10.1029/2002JD002051, 2002.

871 Varutbangkul, V., Brechtel, F. J., Bahreini, R., Ng, N. L., Keywood, M. D., Kroll, J. H., Flagan,  
872 R. C., Seinfeld, J. H., Lee, A., and Goldstein, A. H.: Hygroscopicity of secondary organic  
873 aerosols formed by oxidation of cycloalkenes, monoterpenes, sesquiterpenes, and related

874 compounds, *Atmos. Chem. Phys.*, 6, 2367–2388, <http://www.atmos-chem-phys.net/6/23>  
875 67/2006/, 2006.

876 Veghte, D. P., Altaf, M. B., and Freedman, M. A.: Size dependence of the structure of organic  
877 aerosol, *J. Am. Chem. Soc.*, 135, 16046–16049, 2013.

878 Wang, G., Zhang, R., Gomez, M. E., Yang, L., Zamora, M. L., Hu, M., Lin, Y., Peng, J., Guo, S.,  
879 and Meng, J.: Persistent sulfate formation from London Fog to Chinese haze, *Proc. Natl. Acad.  
880 Sci. U. S. A.*, 113, 13630–13635, 2016.

881 Wang, S., Ye, J., Soong, R., Wu, B., Yu, L., Simpson, A. J., and Chan, A. W. H.: Relationship  
882 between chemical composition and oxidative potential of secondary organic aerosol from  
883 polycyclic aromatic hydrocarbons, *Atmos. Chem. Phys.*, 18, 3987–4003, 2018.

884 Wang, S., Zhou, S., Tao, Y., Tsui, W. G., Ye, J., Yu, J. Z., Murphy, J. G., McNeill, V. F.,  
885 Abbatt, J. P. D., and Chan, A. W. H.: Organic peroxides and sulfur dioxide in aerosol: Source of  
886 particulate sulfate, *Environ. Sci. Technol.*, 53, 10695–10704, 10.1021/acs.est.9b02591, 2019.

887 Wang, X.; Gemayel, R.; Hayeck, N.; Perrier, S.; Charbonnel, N.; Xu, C.; Chen, H.; Zhu, C.;  
888 Zhang, L.; Wang, L.; Nizkorodov, S. A.; Wang, X.; Wang, Z.; Wang, T.; Mellouki, A.; Riva, M.;  
889 Chen, J.; George, C. Atmospheric photosensitization: A new pathway for sulfate formation,  
890 *Environ. Sci. Technol.*, 54, 3114–3120, 2020.

891 Wang, Y., Zhang, Q., Jiang, J., Zhou, W., Wang, B., He, K., Duan, F., Zhang, Q., Philip, S., and  
892 Xie, Y.: Enhanced sulfate formation during China's severe winter haze episode in January 2013  
893 missing from current models, *J. Geophys. Res. Atmos.*, 119, 10425–10440, 2014.

894 Wei, H., Vejerano, E. P., Leng, W., Huang, Q., Willner, M. R., Marr, L. C., and Vikesland, P. J.:  
895 Aerosol microdroplets exhibit a stable pH gradient, *Proc. Natl. Acad. Sci. U. S. A.*, 115, 7272,  
896 10.1073/pnas.1720488115, 2018.

897 Xu, L., Guo, H., Boyd, C. M., Klein, M., Bougiatioti, A., Cerully, K. M., Hite, J. R., Isaacman-  
898 VanWertz, G., Kreisberg, N. M., and Knote, C.: Effects of anthropogenic emissions on aerosol  
899 formation from isoprene and monoterpenes in the southeastern United States, *Proc. Natl. Acad.  
900 Sci. U. S. A.*, 112, 37–42, 2015.

901 Yang, Y., Wang, H., Smith, S. J., Easter, R., Ma, P.-L., Qian, Y., Yu, H., Li, C., and Rasch, P. J.:  
902 Global source attribution of sulfate concentration and direct and indirect radiative forcing,  
903 *Atmos. Chem. Phys.*, 17, 8903–8922, <https://doi.org/10.5194/acp17-8903-2017>, 2017.

904 Yao, M., Zhao, Y., Hu, M., Huang, D., Wang, Y.C., Yu, J. Z., and Yan, N.: Multiphase reactions  
905 between secondary organic aerosol and sulfur dioxide: kinetics and contributions to sulfate  
906 formation and aerosol aging, *Environ. Sci. Tech. Let.* 6, 768–774, 2019.

907 Ye, J., Gordon, C. A., and Chan, A. W. H.: Enhancement in secondary organic aerosol formation  
908 in the presence of preexisting organic particle, *Environ. Sci. Technol.*, 50, 3572–3579, 2016.

909 Ye, J., Abbatt, J. P. D., and Chan, A. W. H.: Novel pathway of SO<sub>2</sub> oxidation in the atmosphere:  
910 reactions with monoterpene ozonolysis intermediates and secondary organic aerosol, *Atmos.  
911 Chem. Phys.*, 18, 5549–5565, <https://doi.org/10.5194/acp18-5549-2018>, 2018.

912 Yee, L. D., Isaacman-VanWertz, G., Wernis, R. A., Kreisberg, N. M., Glasius, M., Riva, M.,  
913 Surratt, J. D., de Sá, S. S., Martin, S. T., Alexander, M. L., Palm, B. B., Hu, W., Campuzano-  
914 Jost, P., Day, D. A., Jimenez, J. L., Liu, Y., Misztal, P. K., Artaxo, P., Viegas, J., Manzi, A., de

915 Souza, R. A. F., Edgerton, E. S., Baumann, K., and Goldstein, A. H.: Natural and  
916 anthropogenically influenced isoprene oxidation in southeastern United States and central  
917 Amazon, *Environ. Sci. Technol.*, 54, 5980-5991, 10.1021/acs.est.0c00805, 2020.

918 You, Y., Renbaum-Wolff, L., Bertram, A. K.: Liquid-liquid phase separation in particles  
919 containing organics mixed with ammonium sulfate, ammonium bisulfate, ammonium nitrate or  
920 sodium chloride, *Atmos. Chem. Phys.*, 13, 11723–11734, <https://doi.org/10.5194/acp-13-11723-2013>, 2013.

922 You, Y., Smith, M. L., Song, M., Martin, S. T., and Bertram, A. K.: Liquid–liquid phase  
923 separation in atmospherically relevant particles consisting of organic species and inorganic salts,  
924 *Int. Rev. Phys. Chem.*, 33, 43–77, doi:10.1080/0144235X.2014.890786, 2014.

925 Zhang, S., Xing, J., Sarwar, G., Ge, Y., He, H., Duan, F., Zhao, Y., He, K., Zhu, L. and Chu, B.:  
926 Parameterization of heterogeneous reaction of SO<sub>2</sub> to sulfate on dust with coexistence of NH<sub>3</sub>  
927 and NO<sub>2</sub> under different humidity conditions, *Atmos. Environ.*, 208, 133-140, 2019.

928 Zhao, Y., Liu, Y., Ma, J., Ma, Q., and He, H.: Heterogeneous reaction of SO<sub>2</sub> with soot: The  
929 roles of relative humidity and surface composition of soot in surface sulfate formation, *Atmos.*  
930 *Environ.*, 152, 465-476, 2017.

931 Zheng, B., Zhang, Q., Zhang, Y., He, K. B., Wang, K., Zheng, G. J., Duan, F. K., Ma, Y. L., and  
932 Kimoto, T.: Heterogeneous chemistry: a mechanism missing in current models to explain  
933 secondary inorganic aerosol formation during the January 2013 haze episode in North China,  
934 *Atmos. Chem. Phys.*, 15, 2031–2049, doi:10.5194/acp-15-2031-2015, 2015.

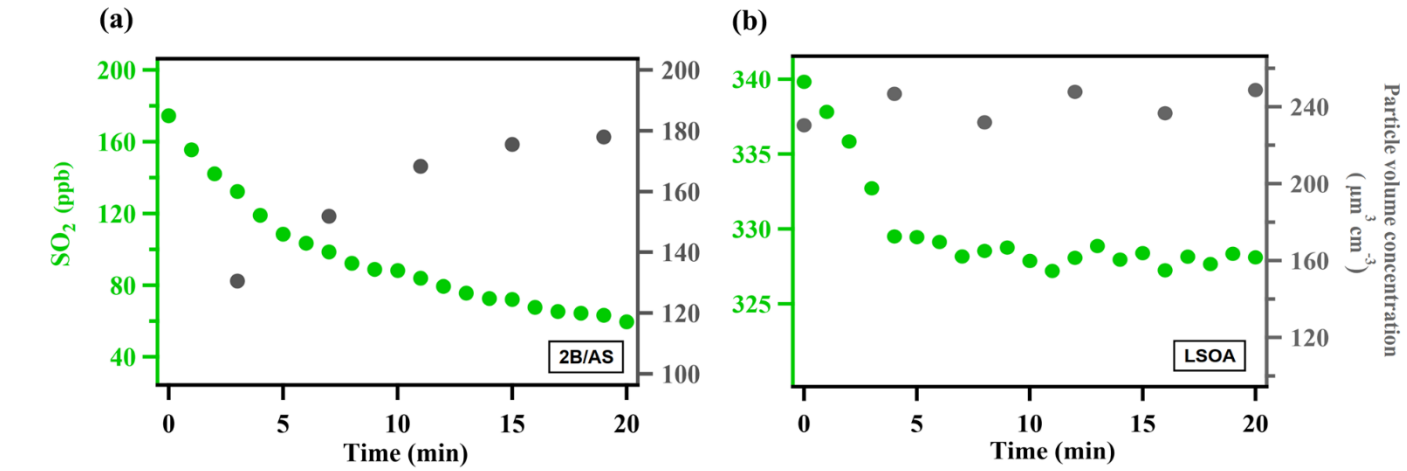
935 Zheng, G. J., Duan, F. K., Su, H., Ma, Y. L., Cheng, Y., Zheng, B., Zhang, Q., Huang, T.,  
936 Kimoto, T., Chang, D., Pöschl, U., Cheng, Y. F., and He, K. B.: Exploring the severe winter haze  
937 in Beijing: the impact of synoptic weather, regional transport and heterogeneous reactions,  
938 *Atmos. Chem. Phys.*, 15, 2969–2983, doi:10.5194/acp-15-2969-2015, 2015.

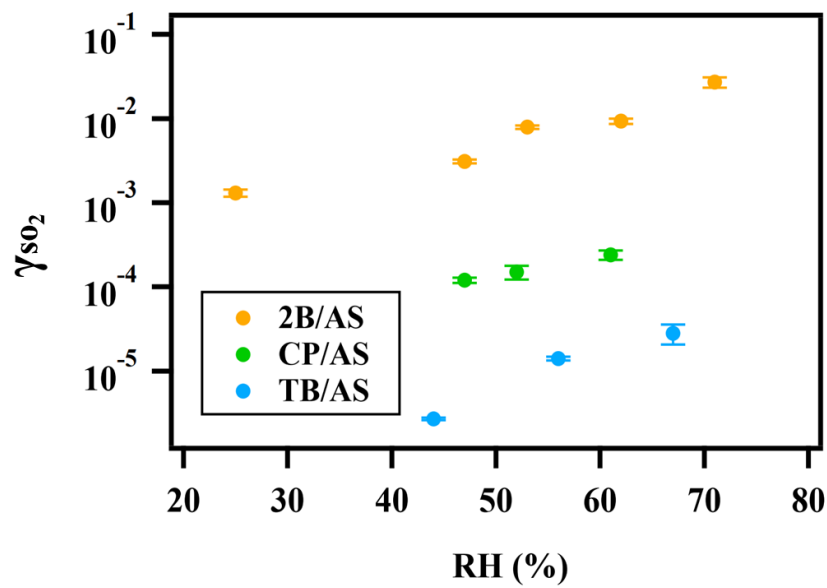
939 Zheng, G., Su, H., Wang, S., Andreae, M. O., Pöschl, U., and Cheng, Y.: Multiphase buffer  
940 theory explains contrasts in atmospheric aerosol acidity, *Science*, 369, 1374-1377,  
941 10.1126/science.aba3719, 2020.

942

943

944





962

963 **Figure 2.** Exponential relationship between  $\gamma_{\text{SO}_2}$  and RH for ammonium sulfate aerosol  
 964 containing 2-butanone peroxide (2B), cumene hydroperoxide (CP), tert-butyl hydroperoxide  
 965 (TB).

966

967

968

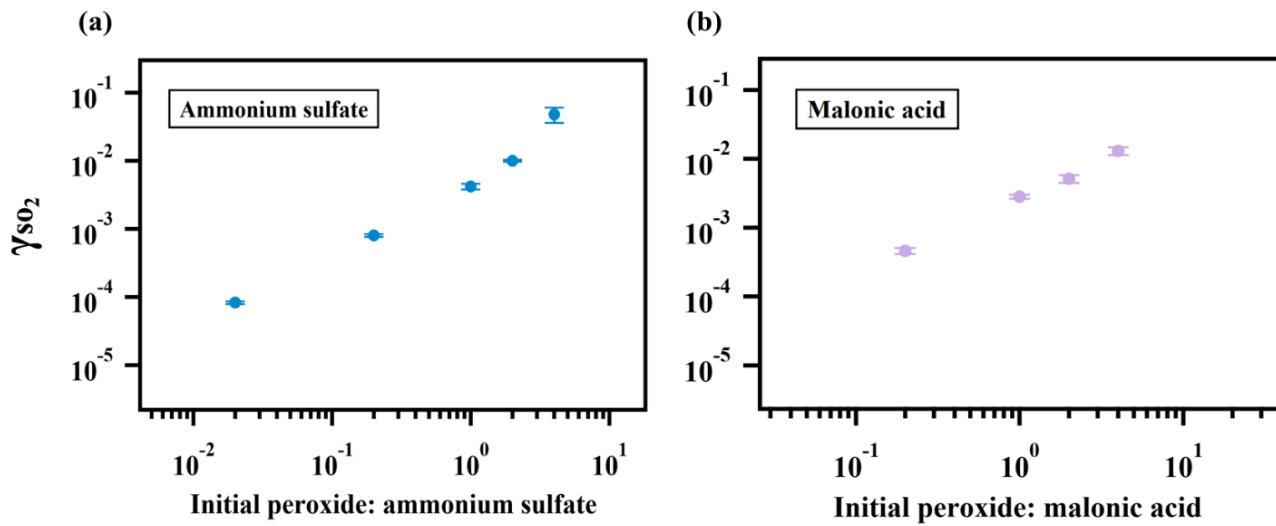
969

970

971

972

973



974

975 **Figure 3.** Relationship between  $\gamma_{\text{SO}_2}$  and particulate peroxide content.  $\gamma_{\text{SO}_2}$  for ammonium sulfate  
976 (a) and malonic acid aerosol (b) containing different amount of 2-butanone peroxide are shown  
977 here. The observed dependence of  $\gamma_{\text{SO}_2}$  on the amount of peroxide injected are linear since the  
978 slopes of the relationship are both nearly 1 in (a) and (b).

979

980

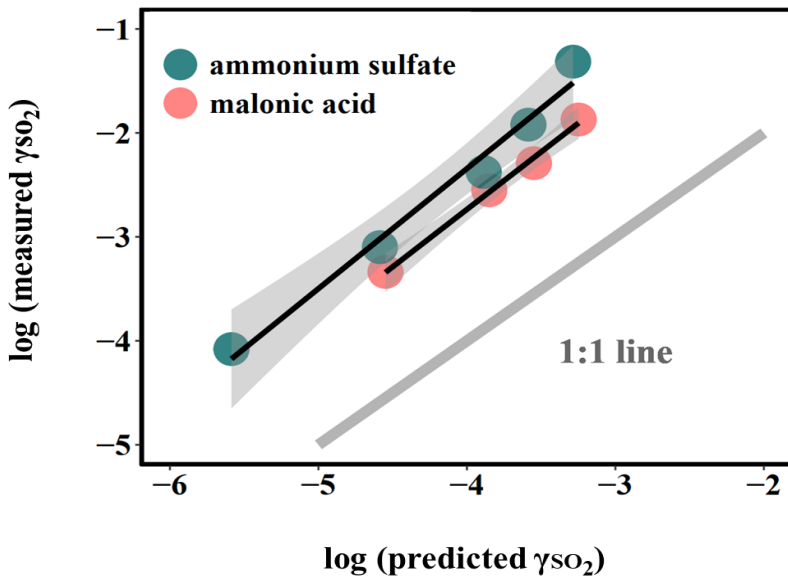
981

982

983

984

985



986

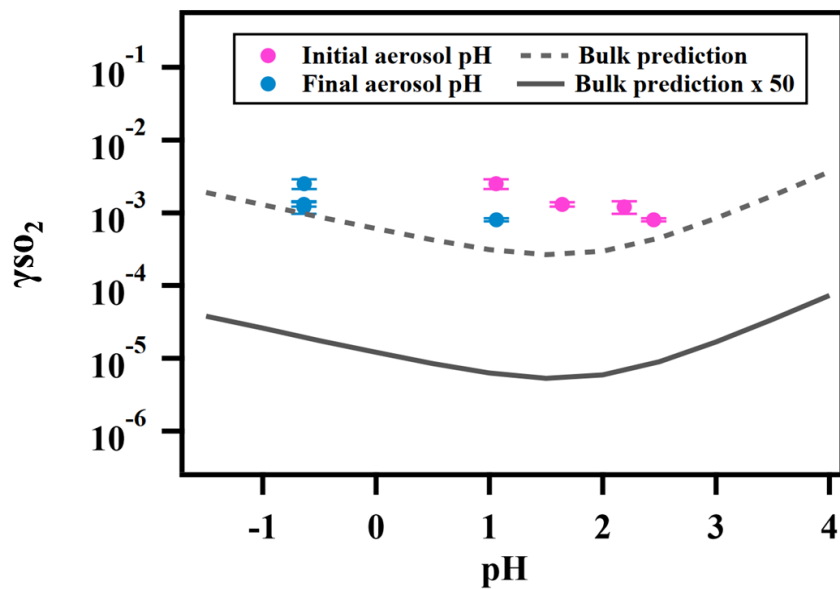
987 **Figure 4.** Relationship between measured  $\gamma_{SO_2}$  and  $\gamma_{SO_2}$  predicted by Eqn. 5. The large deviation  
 988 from the 1:1 line, which represents the difference between the measured uptake coefficient and  
 989 predicted values based on kinetics in the dilute aqueous phase, indicates that aerosol reactive  
 990 uptake is significantly faster than reactions in dilute aqueous phase. This enhancement is likely  
 991 driven in part by high ionic strengths, as the difference between measured  $\gamma_{SO_2}$  and predicted  $\gamma_{SO_2}$   
 992 are consistently higher for organic peroxide containing ammonium sulfate (high ionic strength)  
 993 than for that mixed with malonic acid (lower ionic strength).

994

995

996

997



998

999 **Figure 5.** Relationship between  $\gamma_{\text{SO}_2}$  and aerosol phase pH for ammonium sulfate aerosol

1000 containing 2-butanone peroxide.

1001

1002

1003

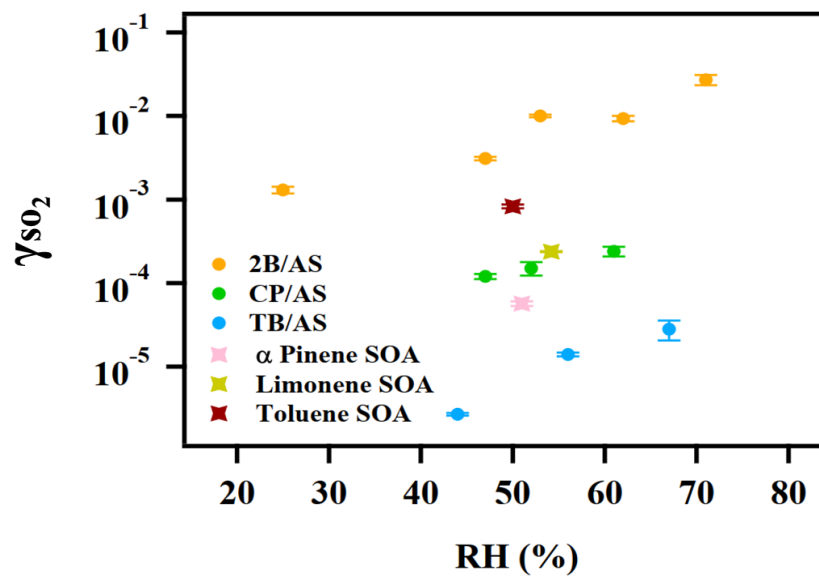
1004

1005

1006

1007

1008



1009

1010 **Figure 6.**  $\gamma_{SO_2}$  measured for different types of organic aerosol. The reactive uptake coefficient of  
 1011  $SO_2$  onto SOA are on the order of  $10^{-4}$ .

1012

1013

1014

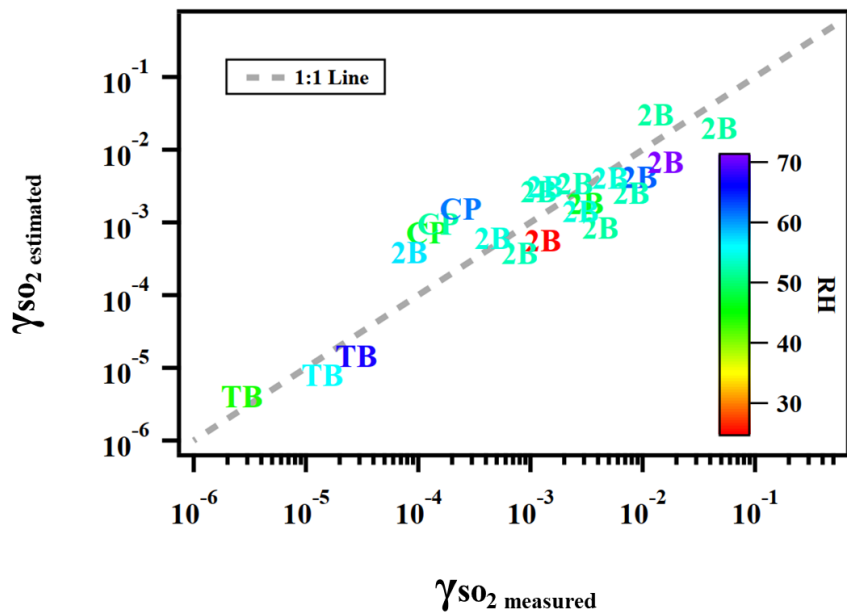
1015

1016

1017

1018

1019



1020

1021 **Figure 7.** Predicted  $\gamma_{SO_2}$  using Equation (13) versus measured  $\gamma_{SO_2}$  for ammonium sulfate or  
 1022 malonic acid aerosol containing 2-butanone peroxide (2B), cumene hydroperoxide (CP), tert-  
 1023 butyl hydroperoxide (TB) under different experimental conditions.

1024

1025

1026

1027

1028

1029

1030